Floquet Driven Superlattice

Simon Wittum

Bachelorarbeit in Physik
angefertigt im Physikalischen Institut

vorgelegt der
Mathematisch-Naturwissenschaftlichen Fakultät
der
Rheinischen Friedrich-Wilhelms-Universität
Bonn

August 2022

Ich versichere, dass ich diese Arbeit selbstständig verfasst und keine anderen als die angegebenen Quellen und Hilfsmittel benutzt sowie die Zitate kenntlich gemacht habe.

Bonn, 1.8.22 ..... S. [illegible]

Datum Unterschrift

1. Gutachterin: Prof. Dr. Corinna Kollath
2. Gutachterin: Dr. Ameneh Sheikhan

Acknowledgements

First of all, I want to thank Prof. Dr. Corinna Kollath for giving me the opportunity to write my bachelor thesis in her research group on a topic that has been very interesting to me.

Furthermore, I would like to express my gratitude towards Dr. Ameneh Sheikhan for her immense support and incredible patience, and for acting as second examiner.

Many thanks also go to the rest of the research group for the motivating atmosphere and the enriching discussions we had during the lunch breaks. Especially, I want to thank Karin Haderlein, Luisa Tolle and Florin Hemmann for sharing the office with me, always helping me out with technical difficulties, and for proof reading this thesis.

Last but not least, I would like to thank my friends and family for their emotional support and encouragements throughout my entire studies.

Contents

CHAPTER 1

Introduction

Over the last decades, the method of Floquet engineering has become increasingly popular. The general idea behind this concept is to systematically change the properties of a quantum mechanical system by adding a time periodic driving force. The time evolution of the driven system is then, apart from a micromotion operator, governed by a time independent effective Hamiltonian whose properties can in principle be very different from those of the Hamiltonian describing the dynamics of the system with no drive. In most applications, one aims to use the driving to taylor the effective Hamiltonian to show some desired features that are not present in the original system [1].

This technique has been applied successfully in various experiments with ultracold atoms in optical lattices. For example, dynamical control of matter wave-tunneling in a driven optical lattice has been achieved experimentally [2–5]. Moreover, the method has been employed to realise photon assisted tunneling [6], Floquet induced superfluid to Mott insulator phase transitions [7], resonant coupling of Bloch bands [8] and the creation of strong artificial magnetic fields [9].

The goal of this thesis is to Floquet engineer a one dimensional superlattice filled with one or two particles to tune its transport parameters. In order to use Floquet engineering, we need to construct the effective Hamiltonian associated to the system. This task is non trivial, urging us to make use of a perturbative approach to derive an approximate expression of the effective Hamiltonian for certain limits. In the one particle case, we do so for the limit of high driving frequencies. In the two particle case, we focus on bound pairs, i.e. the limit of strong coupling, in combination with the high frequency limit. The analytical results can then be compared with solutions obtained with numerical diagonalisation methods, respectively. The thesis will be structured as follows:

- Chapter 2 presents the required theoretical background. First, the Fermi-Hubbard model is introduced. Afterwards, the concept of Floquet theory and its central implications are discussed.
- In chapter 3, the time evolution of a single particle in a superlattice with time periodic driving is investigated.
- Knowing about the single particle dynamics, chapter 4 discusses the time evolution of two on-site interacting particles in the same system.
- Finally, chapter 5 concludes the discussion and gives an outlook of the project.

CHAPTER 2

Theoretical Prerequisites

2.1 Fermi-Hubbard Model

The Fermi-Hubbard model is an attempt to mathematically describe the behaviour of fermions in a spatially periodic potential. It has originally been introduced by John Hubbard in 1963 [10]. The model discretises space, allowing particles to only be located at distinct positions that are energetically favorable[1]. In the formalism of second quantisation, the one dimensional Fermi-Hubbard model for spin-$\frac{1}{2}$-particles reads

$$\hat{H} = -J \sum_{j,\sigma} (\hat{c}^\dagger_{j,\sigma} \hat{c}_{j+1,\sigma} + \text{h.c.}) + U \sum_j \hat{n}_{j,\uparrow} \hat{n}_{j,\downarrow}, \tag{2.1}$$

where j runs over all lattice sites and σ over the two spin states $\{\uparrow, \downarrow\}$. The operators $\hat{c}^\dagger_{j,\sigma}$ and $\hat{c}_{j,\sigma}$ create and annihilate a particle at lattice site j with spin σ, obeying the fermionic anticommutation relations

$$\begin{aligned} \{\hat{c}_{i,\sigma}, \hat{c}_{j,\bar{\sigma}}\} &= \{\hat{c}^\dagger_{i,\sigma}, \hat{c}^\dagger_{j,\bar{\sigma}}\} = 0, \\ \{\hat{c}_{i,\sigma}, \hat{c}^\dagger_{j,\bar{\sigma}}\} &= \delta_{ij} \delta_{\sigma\bar{\sigma}}. \end{aligned} \tag{2.2}$$

From the operators $\hat{c}^\dagger_{j,\sigma}$ and $\hat{c}_{j,\sigma}$, one can construct the number operators $\hat{n}_{j,\sigma} = \hat{c}^\dagger_{j,\sigma} \hat{c}_{j,\sigma}$ that count the number of particles located at site j with spin σ.

The interpretation of eq. (2.1) is straightforward and depicted in fig. 2.1. The first term allows particles to hop from one site to adjacent ones by tunneling through the potential well separating them with a tunneling amplitude J. The second term represents a short range interaction of two particles with different spin that are located on the same site[2]. The influence of this effect is scaled by the interaction amplitude U.

In order to derive the Hamilton operator of the Fermi-Hubbard model, one has to start with the many-body Hamilton operator describing the behaviour of particles in a periodic potential in the language of second quantisation. By expressing the field operators in terms of the localised Wannier functions, sticking to the lowest Bloch band and only considering nearest-neighbour hopping and on-site interactions,

[1] Mathematically, this means that the lattice sites are the positions j where the potential $V(x)$ becomes minimal.

[2] As we are dealing with fermions, the Pauli exclusion principle holds. Therefore, it is not possible for two particles with the same spin to be located on the same site.

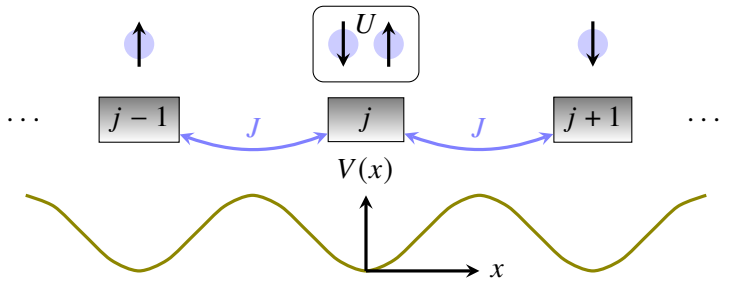

Figure 2.1: Sketch of the 1D Fermi-Hubbard model for spin-$\frac{1}{2}$-particles. Particles are only allowed to be located at discrete lattice sites which are the positions j where the periodic potential $V(x)$ becomes smallest. They are able to jump to adjacent lattice sites by tunneling through the potential well separating them with the tunneling amplitude J. Two particles located on the same site interact with the interaction amplitude U. Due to the Pauli exclusion principle, it is not possible for two particles with the same spin to be located at the same site.

one receives the Fermi-Hubbard Hamiltonian from eq. (2.1) [11]. As long as the temperature of the system is close to absolute zero[3], the results obtained with the Hubbard model are reliable. For higher temperatures, the system becomes more complicated due to thermal effects.

For a given amount of lattice sites L, a suitable basis for the Fock space in which our Hamiltonian operates is given by the eigenstates $\{|n_{1,\uparrow}n_{1,\downarrow}\dots n_{L,\uparrow}n_{L,\downarrow}\rangle\}$ of the number operators, defined by

$$\hat{n}_{j,\sigma}\,|n_{1,\uparrow}n_{1,\downarrow}\dots n_{L,\uparrow}n_{L,\downarrow}\rangle = n_{j,\sigma}\,|n_{1,\uparrow}n_{1,\downarrow}\dots n_{L,\uparrow}n_{L,\downarrow}\rangle\,. \tag{2.3}$$

For fermions, we have $n_{j,\sigma} \in \{0,1\}$. This means that we can identify the numbers in our ket-vectors with binary numbers. In this thesis, we choose the convention of ordering the basis states according to the size of these binary numbers.

Because the Hamiltonian from eq. (2.1) commutes with the total number operator $\hat{N} = \sum_{j,\sigma}\hat{n}_{j,\sigma}$ and the total spin operator $\hat{S} = \sum_j(\hat{n}_{j,\uparrow} - \hat{n}_{j,\downarrow})$, we don't have to work in the full Fock space, but can stay in a subspace $\mathcal{H}^{(N,S)}$ of states with conserved particle number N and total spin S.

2.1.1 Solutions to the Fermi-Hubbard Model

It is not possible to give a general solution to the Fermi-Hubbard Model of eq. (2.1). However, for the two limits $J \gg |U|$ (weak coupling limit) and $|U| \gg J$ (with $U < 0$, strong coupling limit), it is possible to analytically compute the eigenstates and -values.

Weak Coupling Limit

In the weak coupling limit ($J \gg |U|$), we can drop the interaction term in eq. (2.1) and the system factorises into the single particle solutions. In order to find the single particle solutions, one can diagonalise the Hamiltonian by expressing it in momentum space, i. e. taking its Fourier transform. The

[3] To be more precise, this means that the thermal energy of the system is significantly smaller than the energy scales of the hopping and the interaction. Generally, this is only realised for temperatures close to absolute zero.

solutions are free waves

$$\left|\psi_{k_n}\right\rangle = \mathcal{N} \sum_{j=1}^{L} \mathrm{e}^{\mathrm{i}k_n j} \left|j\right\rangle, \tag{2.4}$$

where the expression $|j\rangle = \hat{c}_j^\dagger |\Omega\rangle$[4] is the shorthand notation for a particle localised at site j[5] and $\mathcal{N}$ a normalisation constant. Note that in the entire thesis, we are working in units where the spatial periodicity a of the lattice is 1. The momenta k_m can only take the discrete values

$$k_m = \frac{2\pi}{L} m \quad \text{with} \quad m \in \{1, \ldots, L\}. \tag{2.5}$$

The eigenvalues corresponding to the eigenstates displayed in eq. (2.4) are given by

$$E(k_m) = -2J \cos(k_m). \tag{2.6}$$

For a more detailed discussion, see e.g. [11].

Strong Coupling Limit

For the strong coupling limit ($\alpha = J/|U| \ll 1$ with $U < 0$), by performing a so-called Schrieffer-Wolff Transformation, it can be shown ([11]) that up to some irrelevant constant extra terms, the Hamiltonian from eq. (2.1) can be written as

$$\hat{H}_{\mathrm{SC}} = -\frac{2J^2}{|U|} \sum_j (\hat{\eta}_j^+ \hat{\eta}_{j+1}^- + \mathrm{h.c.}) + O\left(\alpha^3\right), \tag{2.7}$$

where η_j^+ and η_j^- are the "creation" and "annihilation" operators for pairs defined as

$$\begin{aligned} \hat{\eta}_j^+ &= \hat{c}_{j,\uparrow}^\dagger \hat{c}_{j,\downarrow}^\dagger \\ \hat{\eta}_j^- &= \hat{c}_{j,\uparrow} \hat{c}_{j,\downarrow}. \end{aligned} \tag{2.8}$$

However, these operators are no real creation and annihilation operators by definition as they do not obey the fermionic anticommutation relations from eq. (2.2). Instead, they are part of a spin-$\frac{1}{2}$-algebra[6] together with the operator

$$\hat{\eta}_i^z = (\hat{n}_{i,\uparrow} + \hat{n}_{i,\downarrow} - 1)/2. \tag{2.9}$$

The new Hamiltonian can be understood quite intuitively. Due to the strong coupling, the particles tend to stick together and move in pairs. Therefore, our new Hamiltonian describes an effective "Pair-particle" with a kinetic part only, where the pair hopping amplitude is given by

$$J^{\mathrm{p}} = \frac{2J^2}{|U|}. \tag{2.10}$$

[4] We label the vacuum state with $|\Omega\rangle$ because $|0\rangle = \hat{c}_0^\dagger |\Omega\rangle$ already represents a particle at site 0.

[5] This notation can only be used for one particle states. When we are dealing with one particle problems, we will stick to this labelling. In all other cases, we use the notation introduced above.

[6] The meaning of this will be explained in the appendix in chapter A.

Hence, the solutions are again given by the standing waves from eq. (2.4), with the eigenenergies

$$E(k_m) = -J^{\mathrm{p}} \cos(k_m), \tag{2.11}$$

where we replaced J in eq. (2.6) by the pair hopping amplitude J^{p}.

2.1.2 Dynamics

So far, we only talked about the stationary solutions of the Hubbard model. We now take a look at the time evolution of different states.

Two Site Oscillations

First, let us consider the two site model filled with one particle only. Later in the thesis, we are going to introduce the staggered potential

$$\hat{H}_\Delta = \Delta \sum_{j,\sigma} (-1)^j \hat{n}_{j,\sigma} \tag{2.12}$$

to our model. In order to save some time, we will already consider it in this derivation. Note that we can go back to the original model any time by setting $\Delta = 0$. In the basis $\{|1\rangle, |2\rangle\}$, our Hamilton operator then reads[7]

$$\hat{H} \doteq \begin{pmatrix} -\Delta & -J \\ -J & \Delta \end{pmatrix}. \tag{2.13}$$

We let our particle start at the first site, i.e. $|\psi(t_0)\rangle = |1\rangle$. Using the time evolution operator $\hat{U}(t, t_0)$, we evolve our state in time and get

$$\begin{aligned} |\psi(t)\rangle &= \hat{U}(t, t_0) |\psi(t_0)\rangle = \exp\left(-\mathrm{i}\frac{t - t_0}{\hbar}\hat{H}\right) |\psi(t_0)\rangle \\ &= \left\{ \cos\left(\frac{\sqrt{J^2 + \Delta^2}}{\hbar} t\right) + \frac{\mathrm{i}\Delta}{\sqrt{J^2 + \Delta^2}} \sin\left(\frac{\sqrt{J^2 + \Delta^2}}{\hbar} t\right) \right\} |1\rangle + \frac{\mathrm{i}J}{\sqrt{J^2 + \Delta^2}} \sin\left(\frac{\sqrt{J^2 + \Delta^2}}{\hbar} t\right) |2\rangle . \end{aligned} \tag{2.14}$$

For the expectation value of the number operators, we find

$$\langle \hat{n}_1 \rangle(t) = \langle \psi(t) | \hat{n}_1 | \psi(t) \rangle = \frac{J^2/2 + \Delta^2}{J^2 + \Delta^2} + \frac{J^2/2}{J^2 + \Delta^2} \cos\left(2\frac{\sqrt{J^2 + \Delta^2}}{\hbar} t\right), \tag{2.15}$$

$$\langle \hat{n}_2 \rangle(t) = \langle \psi(t) | \hat{n}_2 | \psi(t) \rangle = \frac{J^2/2}{J^2 + \Delta^2} - \frac{J^2/2}{J^2 + \Delta^2} \cos\left(2\frac{\sqrt{J^2 + \Delta^2}}{\hbar} t\right). \tag{2.16}$$

Because $\langle \hat{n}_j \rangle$ indicates the probability that the particle is located at site j, we interpret it as probability density. The results of eq. (2.15) and (2.16) then correspond to a particle oscillating between two sites with the frequency

$$\Omega(\Delta) = \frac{2\sqrt{J^2 + \Delta^2}}{\hbar}. \tag{2.17}$$

[7] As we are dealing with one particle only, we can drop the interaction term of eq. (2.1).

We see that for $\Delta \to \infty$, we get $\langle \hat{n}_1 \rangle(t) \equiv 1$ and $\langle \hat{n}_2 \rangle(t) \equiv 0$, implying that the particle will stay located at lattice site 1 for all times.

Particle Propagation in the 1D-lattice

In the 1D-lattice described by the Fermi-Hubbard model, the velocity of a particle with momentum k_m can be calculated from eq. (2.6) by

$$v(k_m) = \left.\frac{\partial E(k)}{\partial k}\right|_{k=k_m} = 2J \sin(k_m). \tag{2.18}$$

Due to the Heisenberg uncertainty principle, the momentum of a particle localised at site j is unknown. Using the Fourier representation of the creation operators, we can write

$$\left|\psi(t_0)\right\rangle = |j\rangle = \hat{c}_j^\dagger |\Omega\rangle = \frac{1}{\sqrt{N}} \sum_{m=1}^{L} \mathrm{e}^{\mathrm{i}k_m j} \hat{c}_{k_m}^\dagger |\Omega\rangle , \tag{2.19}$$

where $\hat{c}_{k_m}^\dagger$ creates a particle with momentum k_m. The spatial standard deviation σ of a particle in the initial state $\left|\psi(t_0)\right\rangle$ linearly increases in time, where the slope is proportional to the velocity of a single Fourier mode. Due to eq. (2.18), we know that $v(k) \propto J$ and therefore, we conclude that

$$\sigma \propto Jt. \tag{2.20}$$

Hence, we see that by studying the delocalisation of a particle over the lattice as a function of time, it is possible to find the hopping amplitude up to a constant scaling.

2.2 Floquet Theory

At this point, we have discussed everything we need to know about the Fermi-Hubbard model to describe the behaviour of fermions in an optical lattice that does not change in time. If we wish to manipulate the lattices features, a relatively easy way to do so is given by the concept of Floquet engineering, which is based on a mathematical theorem originally proposed by Gaston Floquet in 1883 [12]. For our purposes, it can be formulated as follows.

Theorem 1 *The solutions to the time dependent Schrödinger equation for a Hamilton operator that is periodic in time, i.e. $\hat{H}(t+T) = \hat{H}(t)$, can be expressed as*

$$\left|\psi_n(t)\right\rangle = \mathrm{e}^{-i\epsilon_n t/\hbar} \left|u_n(t)\right\rangle , \tag{2.21}$$

where ϵ_n are called the quasi-energies of the state and $\left|u_n(t)\right\rangle = \left|u_n(t+T)\right\rangle$ are the T-periodic Floquet modes.

In order to gain some intuition for this theorem, we first derive this statement and then give some details about its implications. In our presentation, we closely follow [13]. For a different approach, see e.g. [14].

2.2.1 Proof of the Statement

The time evolution operator $\hat{U}(t, t_0)$ by definition is unitary and obeys the composition rule property $\hat{U}(t_1 + t_2, 0) = \hat{U}(t_1 + t_2, t_1)\hat{U}(t_1, 0)$ and the time dependent Schrödinger equation

$$\mathrm{i}\hbar \frac{\partial}{\partial t}\hat{U}(t, t_0) = \hat{H}(t)\hat{U}(t, t_0) \tag{2.22}$$

with the initial condition $\hat{U}(t_0, t_0) = \mathbb{1}$. Because

$$\begin{aligned} \mathrm{i}\hbar \frac{\partial}{\partial t}\hat{U}(t+T, t_0+T) &= \mathrm{i}\hbar \frac{\partial}{\partial t}\hat{U}(t+T, t_0)\hat{U}(t_0, t_0+T) \\ &= \hat{H}(t+T)\hat{U}(t+T, t_0)\hat{U}(t_0, t_0+T) \\ &= \hat{H}(t)\hat{U}(t+T, t_0+T) \end{aligned} \tag{2.23}$$

and $\hat{U}(t_0 + T, t_0 + T) = \mathbb{1}$, the operator $\hat{U}(t + T, t_0 + T)$ satisfies the same differential equation and initial condition as $\hat{U}(t, t_0)$, implying

$$\hat{U}(t + T, t_0 + T) = \hat{U}(t, t_0). \tag{2.24}$$

We will now take a look at the eigenstates $\left|\psi_n(t_0)\right\rangle$ of the time evolution operator over one period $\hat{U}(t_0 + T, t_0)$ at time t_0, which by definition satisfy

$$\hat{U}(t_0 + T, t_0)\left|\psi_n(t_0)\right\rangle = a_n(t_0)\left|\psi_n(t_0)\right\rangle. \tag{2.25}$$

By letting $\hat{U}(t + T, t_0 + T) = \hat{U}(t, t_0)$ act on both sides of eq. (2.25) and inserting $\mathbb{1} = \hat{U}(t_0, t)\hat{U}(t, t_0)$ on the left hand side, we see

$$\begin{aligned} \underbrace{\hat{U}(t+T, t_0+T)\hat{U}(t_0+T, t_0)}_{=\hat{U}(t+T, t_0)}\left|\psi_n(t_0)\right\rangle &= \underbrace{\hat{U}(t+T, t_0)\hat{U}(t_0, t)}_{=\hat{U}(t+T, t)}\underbrace{\hat{U}(t, t_0)\left|\psi_n(t_0)\right\rangle}_{=\left|\psi_n(t)\right\rangle} \\ &= a_n(t_0)\left|\psi_n(t)\right\rangle. \end{aligned} \tag{2.26}$$

This shows that the eigenstates $\left|\psi_n(t)\right\rangle$ of the time evolution operator $\hat{U}(t + T, t)$ are connected to the eigenstates $\left|\psi_n(t_0)\right\rangle$ of $\hat{U}(t_0 + T, t_0)$ by the time evolution operator $\hat{U}(t, t_0)$, implying that the eigenstates of $\hat{U}(t + T, t)$ are solutions to the time dependent Schrödinger equation. Furthermore, we see that the eigenvalues obey $a(t) = a(t_0)$ for all t and thus do not depend on time. Because $\hat{U}(t + T, t)$ is unitary, we can write $a_n = \mathrm{e}^{-\mathrm{i}\epsilon_n T/\hbar}$, so that we have

$$\hat{U}(t + T, t)\left|\psi_n(t)\right\rangle = \left|\psi_n(t + T)\right\rangle = \mathrm{e}^{-\mathrm{i}\epsilon_n T/\hbar}\left|\psi_n(t)\right\rangle. \tag{2.27}$$

We can now formally construct the states $\left|u_n(t)\right\rangle = \mathrm{e}^{\mathrm{i}\epsilon_n t/\hbar}\left|\psi_n(t)\right\rangle$, which are T-periodic as we see from eq. (2.27). Therefore, we can decompose $\left|\psi_n(t)\right\rangle$ as

$$\left|\psi_n(t)\right\rangle = \mathrm{e}^{-\mathrm{i}\epsilon_n t/\hbar}\left|u_n(t)\right\rangle, \tag{2.28}$$

proving the Floquet theorem. In the following, we will refer to $\left|\psi_n(t)\right\rangle$ as the Floquet states, which should not be confused with the Floquet modes $\left|u_n(t)\right\rangle$. Note that due to the unitarity of $\hat{U}(t + T, t)$, the

Floquet states and modes form an orthonormal basis of our Hilbert space, respectively[8].

2.2.2 Implications

Using the completeness of the Floquet states, we can express the time evolution operator $\hat{U}(t_2, t_1)$ as

$$\hat{U}(t_2, t_1) = \sum_n \mathrm{e}^{-\mathrm{i}\epsilon_n (t_2 - t_1)/\hbar} \left|u_n(t_2)\right\rangle \left\langle u_n(t_1)\right| . \tag{2.29}$$

The time evolution of an arbitrary initial state $\left|\psi(t_0)\right\rangle$ is then given by

$$|\psi(t)\rangle = \sum_n c_n \mathrm{e}^{-\mathrm{i}\epsilon_n (t - t_0)/\hbar} \left|u_n(t)\right\rangle \tag{2.30}$$

with the expansion coefficients $c_n = \left\langle u_n(t_0)\middle|\psi(t_0)\right\rangle$. If we place our initial state in a single Floquet state, i.e. $c_n = \delta_{n,n_0}$, the time evolution is (apart from an irrelevant phase factor) T-periodic. However, if the system is prepared in a coherent superposition of different Floquet states, we have two contributions to the time evolution. The first is caused by the T-periodic evolution of the Floquet modes $\left|u_n(t)\right\rangle$ which we refer to as the micromotion. The second contribution stems from the relative dephasing of the factors $\mathrm{e}^{-\mathrm{i}\epsilon_n t/\hbar}$, causing a deviation from the periodic evolution of the micromotion.

If we wish to study the time evolution of our system for time scales that are large compared to T, we can neglect the micromotion and investigate our system in a stroboscopic fashion. The stroboscopic time evolution is described by a time independent Floquet Hamiltonian, defined by the full cycle time evolution operator

$$\exp\left(-\frac{\mathrm{i}}{\hbar} T \hat{H}^{\mathrm{F}}_{t_0}\right) \equiv \hat{U}(t_0 + T, t_0). \tag{2.31}$$

The Floquet Hamiltonian by construction is diagonal in the basis of the Floquet modes $\left|u_n(t_0)\right\rangle$ with eigenvalues ϵ_n, making it possible to write

$$\hat{H}^{\mathrm{F}}_{t_0} = \sum_n \epsilon_n \left|u_n(t_0)\right\rangle \left\langle u_n(t_0)\right| . \tag{2.32}$$

This means that we can obtain the Floquet modes and the quasienergy spectrum by diagonalising the Floquet Hamiltonian. The relations $\hat{H}^{\mathrm{F}}_{t_0'} = \hat{U}^{\dagger}(t_0, t_0')\hat{H}^{\mathrm{F}}_{t_0}\hat{U}(t_0, t_0')$ and $\hat{H}^{\mathrm{F}}_{t_0+T} = \hat{H}^{\mathrm{F}}_{t_0}$ can be easily deduced from the explicit representation of $\hat{H}^{\mathrm{F}}_{t_0}$ in eq. (2.32).

Analogously, the micromotion is described by the micromotion operator, which can be expressed as

$$\hat{U}_{\mathrm{micro}}(t_2, t_1) = \sum_n \left|u_n(t_2)\right\rangle \left\langle u_n(t_1)\right| , \tag{2.33}$$

so that it evolves a Floquet mode in time. The total time evolution operator is then connected to the Floquet Hamiltonian and the mircomotion operator by

$$\hat{U}(t_2, t_1) = \mathrm{e}^{-\mathrm{i}(t_2 - t_1)\hat{H}^{\mathrm{F}}_{t_2}/\hbar} \hat{U}_{\mathrm{micro}}(t_2, t_1) = \hat{U}_{\mathrm{micro}}(t_2, t_1) \mathrm{e}^{-\mathrm{i}(t_2 - t_1)\hat{H}^{\mathrm{F}}_{t_1}/\hbar}. \tag{2.34}$$

[8] It should be known to the reader that the eigenbasis of a hermitean operator forms a complete orthonormal basis of the corresponding Hilbert space. It can be shown that this holds for unitary operators as well, see chapter B in the appendix.

The Effective Hamiltonian

It can be shown that for any T-periodic Hamilton operator $\hat{H}(t)$, there exists a unitary gauge transformation $\hat{U}_{\mathrm{F}}(t)$ that transforms $\hat{H}(t)$ into a time independent operator $\hat{H}_{\mathrm{F}}$ that describes the dynamics in the transformed system. This operator is referred to as the effective Hamiltonian. The time evolution can now be computed by transforming to the new system, letting $\hat{H}_{\mathrm{F}}$ mediate the time translation, and then transforming back to the original system, as expressed by

$$\hat{U}(t,t_0) = \hat{U}_{\mathrm{F}}(t)\exp\left(-\mathrm{i}(t-t_0)\hat{H}_{\mathrm{F}}/\hbar\right)\hat{U}_{\mathrm{F}}^{\dagger}(t_0). \tag{2.35}$$

In order to see the connection to the Floquet Hamiltonian $\hat{H}_{t_0}^{\mathrm{F}}$ and the micromotion operator $\hat{U}_{\mathrm{micro}}(t,t_0)$, we insert $\mathbb{1} = \hat{U}_{\mathrm{F}}^{\dagger}(t_0)\hat{U}_{\mathrm{F}}(t_0)$ on the right hand side of eq. (2.35) to get

$$\hat{U}(t,t_0) = \hat{U}_{\mathrm{F}}(t)\hat{U}_{\mathrm{F}}^{\dagger}(t_0)\exp\left(-\mathrm{i}(t-t_0)\hat{U}_{\mathrm{F}}(t_0)\hat{H}_{\mathrm{F}}\hat{U}_{\mathrm{F}}^{\dagger}(t_0)/\hbar\right). \tag{2.36}$$

Comparing this to the right side of eq. (2.34), we see that

$$\hat{U}_{\mathrm{micro}}(t,t_0) = \hat{U}_{\mathrm{F}}(t)\hat{U}_{\mathrm{F}}^{\dagger}(t_0) \tag{2.37}$$

$$\hat{H}_{t_0}^{\mathrm{F}} = \hat{U}_{\mathrm{F}}(t_0)\hat{H}_{\mathrm{F}}\hat{U}_{\mathrm{F}}^{\dagger}(t_0). \tag{2.38}$$

This means that $\hat{H}_{\mathrm{F}}$ and $\hat{H}_{t_0}^{\mathrm{F}}$ are related by a unitary transformation. However, the gauge can in some cases be chosen in a way so that they both coincide. The crucial advantage of working with the effective Hamiltonian rather than the Floquet Hamiltonian is that it does not even depend on time parametrically.

2.2.3 High-Frequency Approximation

In general, it is neither a trivial task to exactly solve a Floquet driven system, nor to find a gauge transformation $\hat{U}_{\mathrm{F}}(t)$ that leads to the effective Hamiltonian. However, it is possible to expand the effective Hamiltonian $\hat{H}_{\mathrm{F}}$ in powers of the inverse driving frequency $\omega = 2\pi/T$, i.e.

$$\hat{H}_{\mathrm{F}}(t) = \sum_{n=0}^{\infty}\hat{H}_{\mathrm{F}}^{(n)}, \tag{2.39}$$

where the ω-dependency has been absorbed in the $\hat{H}_{\mathrm{F}}^{(n)}$ terms. The first order terms of this expansion can be calculated by (cf. [13])

$$\begin{aligned}
\hat{H}_{\mathrm{F}}^{(0)} &= \hat{H}_0 \\
\hat{H}_{\mathrm{F}}^{(1)} &= \sum_{m=1}^{\infty}\frac{[\hat{H}_m,\hat{H}_{-m}]}{m\hbar\omega} \\
\hat{H}_{\mathrm{F}}^{(2)} &= \sum_{m\neq 0}\left(\frac{[\hat{H}_{-m},[\hat{H}_0,\hat{H}_m]]}{2(m\hbar\omega)^2} + \sum_{m'\neq 0,m}\frac{[\hat{H}_{-m'},[\hat{H}_{m'-m},\hat{H}_m]]}{3mm'(\hbar\omega)}\right),
\end{aligned} \tag{2.40}$$

where the $\hat{H}_m$ terms are the Fourier components of the original Hamiltonian given by

$$\hat{H}_m = \frac{1}{T}\int_0^T \mathrm{d}t \hat{H}(t)\mathrm{e}^{-\mathrm{i}m\omega t}. \tag{2.41}$$

If we consider the energy $\hbar\omega$ associated with the driving frequency to be much bigger than all of the energy scales of $\hat{H}(t)$, one can obtain good results by truncating the expansion after a finite order. However, we later want the driving amplitude to have the same order as the driving frequency. To clarify, we write

$$\hat{H}(t) = \hat{H}_\mathrm{S} + \hat{V}(t), \tag{2.42}$$

where $\hat{H}_\mathrm{S}$ describes the static system without drive and $\hat{V}(t)$ represents the T-periodic driving. If the energy scale of $\hat{V}(t)$ has the same order as $\hbar\omega$, we can see that all of the terms in eq. (2.40) contribute with the same order. This is also true for the higher order terms, which is why it is not reasonable anymore to truncate the expansion in eq. (2.39). In order to solve this problem, one applies the unitary gauge transformation $\hat{U}_\mathrm{D}(t)$[9] to the system, where the Hamilton operator $\hat{H}$ and the states $|\psi(t)\rangle$ transform like

$$\hat{H}(t) \to \hat{H}_\mathrm{D}(t) = \hat{U}_\mathrm{D}^\dagger(t)\hat{H}(t)\hat{U}_\mathrm{D}(t) - \mathrm{i}\hbar\hat{U}_\mathrm{D}^\dagger(t)\left(\frac{\mathrm{d}}{\mathrm{d}t}\hat{U}_\mathrm{D}(t)\right) \tag{2.43}$$

$$|\psi(t)\rangle \to \left|\psi_\mathrm{D}(t)\right\rangle = \hat{U}_\mathrm{D}^\dagger(t)\,|\psi(t)\rangle\,. \tag{2.44}$$

By choosing the gauge to be

$$\hat{U}_\mathrm{D}(t) = \hat{T}\exp\left(\frac{1}{\mathrm{i}\hbar}\int_{t_0}^t \mathrm{d}t'\hat{V}(t') + \phi\right), \tag{2.45}$$

where $\hat{T}$ is the time ordering operator and ϕ an irrelevant phase that can be put to 0, we can make the gauge transformation of the driving term and the second term on the right of eq. (2.43) cancel, so that we end up with

$$\hat{H}_\mathrm{D}(t) = \hat{U}_\mathrm{D}^\dagger(t)\hat{H}_\mathrm{S}\hat{U}_\mathrm{D}(t). \tag{2.46}$$

As we can see, $\hat{H}_\mathrm{D}$ has the same energy scale as $\hat{H}_\mathrm{S}$. Because the gauge transformation operator by construction is T-periodic, $\hat{H}_\mathrm{D}$ is T-periodic as well, which means that we can expand $\hat{H}_\mathrm{D}(t)$ just like $\hat{H}(t)$ in eq. (2.39), where the expansion coefficients can be calculated using eq. (2.40) by replacing $\hat{H}(t)$ with $\hat{H}_\mathrm{D}(t)$. However, as the energy scale of $\hat{H}_\mathrm{D}$ is much smaller than $\hbar\omega$, we are now able to truncate the expansion after a finite order. This means that by applying a unitary transformation, we have brought our Hamilton operator in a form that is more suitable for the high frequency approximation.

Transformation of Operators

In order to avoid confusion, we mention that by applying the unitary transformation $\hat{U}_\mathrm{D}(t)$ to our system, we also need to transform every operator $\hat{O}$ like

$$\hat{O} \to \hat{O}_\mathrm{D} = \hat{U}_\mathrm{D}^\dagger(t)\hat{O}\hat{U}_\mathrm{D}(t), \tag{2.47}$$

[9] Note $\hat{U}_\mathrm{D}(t)$ has nothing to do with the gauge transformation $\hat{U}_\mathrm{F}(t)$ that yields the effective Hamiltonian.

so that the expectation values calculated in the original system coincide with those calculated in the transformed one. We see that if $[\hat{O}, \hat{U}_{\mathrm{D}}(t)] = 0$, we get $\hat{O}_{\mathrm{D}} = \hat{O}$, implying

$$\left\langle \psi_{\mathrm{D}}(t) \middle| \hat{O} \middle| \psi_{\mathrm{D}}(t) \right\rangle = \langle \psi(t) | \hat{O} | \psi(t) \rangle \,. \tag{2.48}$$

In words, this means that for an operator commuting with the gauge, it does not matter whether we calculate the expectation values in the original system or in the transformed one.

CHAPTER 3

One Particle Problem

Having studied the Fermi-Hubbard model and the theoretical toolbox of Floquet theory, it is time to apply those concepts to a system which can be realized in an actual experimental setup. In the following, we consider a modified Fermi-Hubbard model filled with only one particle. The dynamics are described by the kinetic hopping term

$$\hat{H}_J = -J_1 \sum_j (\hat{c}^\dagger_{2j}\hat{c}_{2j+1} + \text{h.c.}) - J_2 \sum_j (\hat{c}^\dagger_{2j+1}\hat{c}_{2j+2} + \text{h.c.}) \tag{3.1}$$

with alternating hopping amplitudes J_1 and J_2. Additionally, we include the parabolic (harmonic oscillator) potential

$$\hat{H}_A = A \sum_j \hat{n}_j j^2 \tag{3.2}$$

in order to trap the particle in the lattice, with A scaling the influence of the trap. The experimental realisation of $\hat{H}_A$ gives an alternating energy offset to the sites, so that the static model needs to be corrected by the staggered term

$$\hat{H}_\Delta = \Delta \sum_j (-1)^j \hat{n}_j, \tag{3.3}$$

where the imbalance Δ indicates the energy shift from the parabola of eq. (3.2). Altogether, the Hamilton operator describing the static system reads

$$\hat{H}_S = \hat{H}_J + \hat{H}_A + \hat{H}_\Delta. \tag{3.4}$$

A visualisation of the model described by eq. (3.4) can be seen in fig. 3.1. For $A = 0$, the Hamilton operator of eq. (3.4) is $2j$-periodic. A system like this is referred to as a superlattice. Therefore, we can think of our Hamiltonian as an effective superlattice described by the kinetic term $\hat{H}_J$ and the staggered term $\hat{H}_\Delta$, upon which an ideal particle trap $\hat{H}_A$ is imposed that does not create an imbalance between the sites.

We wish to alter the dynamics of the superlattice using the concept of Floquet engineering discussed in section 2.2 by adding the time periodic driving term

$$\hat{V}(t) = \frac{V_0}{2} \cos(\omega t) \sum_j (-1)^j \hat{n}_j \tag{3.5}$$

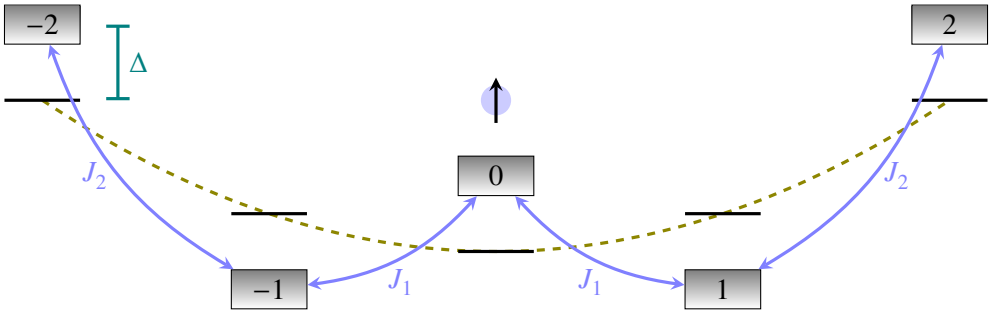

Figure 3.1: Sketch of the one particle model from eq. (3.4). The particle can jump from one site to adjacent ones with the alternating hopping amplitudes J_1 and J_2. In order to trap the particle, a harmonic oscillator potential is imposed to the system. The experimental realisation of the trap gives an additional energetic offset to the sites, displacing them from the parabola in an alternating fashion by the imbalance Δ.

to the static system. The driving can be interpreted as a time periodic oscillation of the energy levels of the lattice sites around their initial level with amplitude $V_0/2$ and (angular) frequency ω, where the oscillation of adjacent sites have a phase shift of π. The Hamilton operator describing the driven system is then given by

$$\hat{H}(t) = \hat{H}_S + \hat{V}(t). \tag{3.6}$$

Before calculating the effective Hamilton operator describing the stroboscopic time evolution in the system, we take a first look at the dynamics created by the Hamilton operator of eq. (3.6).

3.1 Numerical Calculation of the Time Evolution

In order to calculate the time evolution of a given initial state $|\psi(t_0)\rangle$, we have to apply the time evolution operator $\hat{U}(t, t_0)$, which for small time steps $\mathrm{d}t$ can be approximated as

$$\hat{U}(t_0 + \mathrm{d}t, t_0) \approx \exp\left(-\mathrm{i}\frac{\hat{H}(t_0)}{\hbar}\mathrm{d}t\right), \tag{3.7}$$

enabling us to write

$$|\psi(t_0 + \mathrm{d}t)\rangle = \hat{U}(t_0 + \mathrm{d}t, t_0)\,|\psi(t_0)\rangle \approx \exp\left(-\mathrm{i}\frac{\hat{H}(t_0)}{\hbar}\mathrm{d}t\right)|\psi(t_0)\rangle\,. \tag{3.8}$$

The time evolution over a longer time span can then approximately be computed by applying eq. (3.8) multiple times.

First, let us have a look at the two site model. In order to go from the model with L sites of eq. (3.6) to two sites, we need to set $J_2 = 0$. This prevents a particle from escaping a pair of sites connected by J_1. Whenever we talk about a two site model, we set $A = 0$ as the effect of $A \neq 0$ can always be absorbed in $\hat{H}_\Delta$. From eq. (2.17), we know that for a two site model with a kinetic part only, the expectation value of the number operators oscillate with the frequency $\Omega_0 = 2J_1/\hbar$. This corresponds to the period $T_0 = \pi\hbar/J_1$, which we are going to use as a reference time.

In fig. 3.2, we can see the time evolution for a particle starting at the first site. We can see that the

probability density of the particle is oscillating. However, the period of these oscillations is significantly bigger than T_0. Furthermore, by taking a closer look at the oscillations, we can see T-periodic small scale dynamics ($T = 2\pi/\omega$), which we identify with the micromotion. The time evolution of $\langle \hat{H}_J \rangle$ features a T-periodic oscillatory micromotion as well. The amplitude of the micromotion is given by an oscillating envelope with bigger period and amplitude J_1, making the effect of the micromotion very prominent.

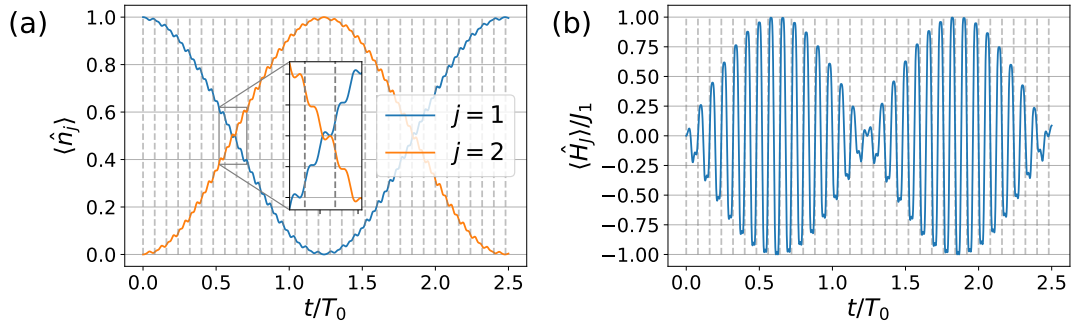

Figure 3.2: Dynamics of the driven two site model with no imbalance filled with one particle. The time evolution of the particle is shown by (a) its location and (b) its kinetic energy. The dashed vertical lines indicate full cycles of the driving given by $2\pi/\omega$. The parameters for both plots are $V_0/(\hbar\omega) = 1.686, \hbar\omega/J_1 = 25$.

Choice of the discretisation parameter

Because most problems that we are dealing with in this thesis are too complicated to be solved analytically, we have to rely on numerical methods several times. Whenever we switch to numerics, we need to discretise continuous variables like time t by a discretisation parameter (also called step width) $\mathrm{d}t$. In order to loose as little information as possible, the discretisation should be chosen very small. However, this also increases the runtime of the program as there is more data to process. In order to find a value for $\mathrm{d}t$ where we can resolve interesting effects, while still having a reasonable program runtime, we always need to check the convergence of our program by comparing the results obtained with different values of $\mathrm{d}t$.

One possibility to check the convergence of the numerics in the context of the two site oscillations is to find the time t_{min} at which the probability for a particle to be at site 1 becomes smallest for the first time. By comparing the results for several values of $\mathrm{d}t$ and analysing for which value we do not see a significant change if we decrease $\mathrm{d}t$ any further, we can find a good choice for the step width. Repeating this procedure in an interval of $\hbar\omega/J_1$, we can make sure that the convergence holds over a wider range.

The analysis yields the results displayed in fig. 3.3. In fig. 3.3 (a), we can see how the procedure works for the parameter choice $\hbar\omega/J_1 = 25$. In fig. 3.3 (b), the convergence over the extended interval $25 \leq \hbar\omega/J_1 \leq 60$ is shown. We see that within the considered range of $\hbar\omega/J_1$, no significant change is happening anymore for stepwidths smaller than $0.001T_0$. Therefore, for this particular example, $\mathrm{d}t = 0.001T_0$ would be an appropriate choice for the discretisation. For $\hbar\omega/J_1 > 30$, reliable results can even be achieved with $\mathrm{d}t = 0.003T_0$.

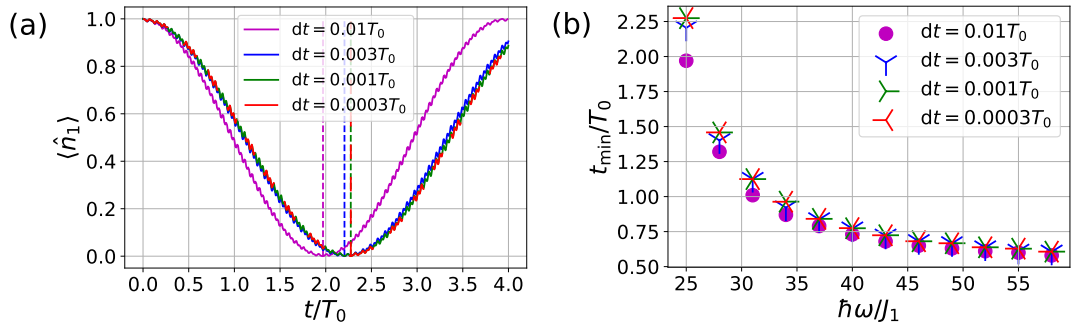

Figure 3.3: Looking at the convergence of the numerics to optimize the choice of the discretisation parameter dt. (a) Demonstration of the convergence for $\hbar\omega/J_1 = 25$ (the vertical lines indicate the time where $\langle \hat{n}_1 \rangle$ becomes minimal) and (b) extension to the range $25 \leq \hbar\omega/J_1 \leq 60$. The parameters are $\Delta/J_1 = 0, V_0/J_1 = 50$.

3.2 High-Frequency Approximation

We now wish to calculate the effective Hamilton operator belonging to the model from eq. (3.6). However, finding its exact form is very complicated, which is why we make use of the high-frequency approximation scheme presented in section 2.2.3. Because we are interested in cases where the amplitude of the driving in eq. (3.5) has the same order as the energy $\hbar\omega$ associated with the driving frequency, the form of the Hamilton operator given in eq. (3.6) is not suitable for the high frequency approximation. Therefore, as discussed in section 2.2.3, we need to find a gauge transformation that satisfies eq. (2.45). In our case, a transformation like that is given by

$$\hat{U}_{\mathrm{D}}(t) = \exp\left(-\mathrm{i}\frac{V_0}{2\hbar\omega}\sin(\omega t)\sum_j (-1)^j \hat{n}_j\right). \tag{3.9}$$

The gauge transformed Hamilton operator $\hat{H}_{\mathrm{D}}(t)$ is then given by

$$\hat{H}_{\mathrm{D}}(t) = \hat{U}_{\mathrm{D}}^{\dagger}(t)\hat{H}_{\mathrm{S}}\hat{U}_{\mathrm{D}}(t).$$

The method used to calculate this expression can be found in the appendix in chapter C. The result is

$$\begin{aligned}\hat{H}_{\mathrm{D}}(t) = &-J_1\sum_j\left(\hat{c}_{2j}^{\dagger}\hat{c}_{2j+1}\mathrm{e}^{\mathrm{i}\frac{V_0}{\hbar\omega}\sin(\omega t)} + \hat{c}_{2j+1}^{\dagger}\hat{c}_{2j}\mathrm{e}^{-\mathrm{i}\frac{V_0}{\hbar\omega}\sin(\omega t)}\right)\\ &-J_2\sum_j\left(\hat{c}_{2j+1}^{\dagger}\hat{c}_{2j+2}\mathrm{e}^{-\mathrm{i}\frac{V_0}{\hbar\omega}\sin(\omega t)} + \hat{c}_{2j+2}^{\dagger}\hat{c}_{2j+1}\mathrm{e}^{\mathrm{i}\frac{V_0}{\hbar\omega}\sin(\omega t)}\right) + \hat{H}_A + \hat{H}_\Delta.\end{aligned} \tag{3.10}$$

Using the Jacobi-Anger expansion (cf. [15] §10.12)

$$\mathrm{e}^{\mathrm{i}z\sin(\phi)} = \sum_{n=-\infty}^{\infty}(-1)^n \mathcal{J}_n(z)\mathrm{e}^{\mathrm{i}n\phi},$$

where $\mathcal{J}_n(z)$ denotes the n-th Bessel function (a sample of the Bessel functions $\mathcal{J}_n(x)$ is illustrated in fig. 3.4) and the parity property

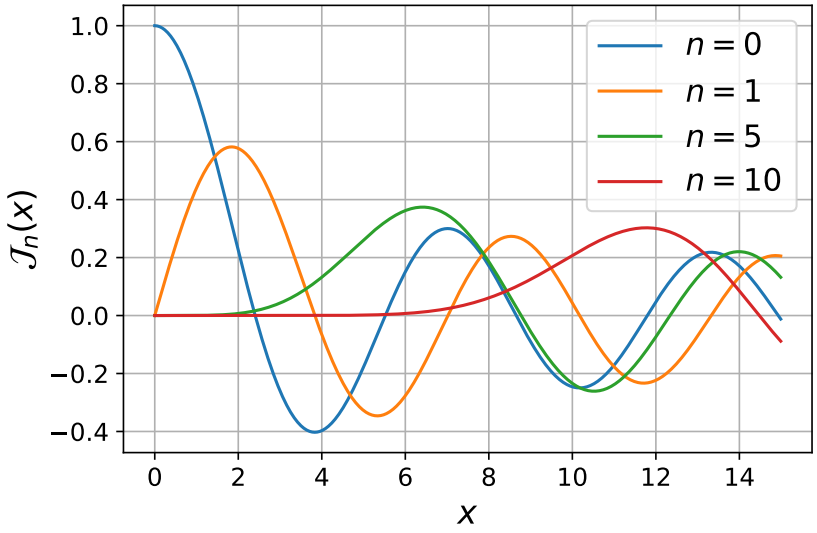

Figure 3.4: Illustration of the Bessel functions $\mathcal{J}_n(x)$ for $n = 0, 1, 5, 10$.

$$\mathcal{J}_n(-x) = (-1)^n \mathcal{J}_n(x) \quad \text{for} \quad n \in \mathbb{Z} \tag{3.11}$$

of the Bessel functions, we find

$$\begin{aligned}\hat{H}_{\mathrm{D}}(t) = -\sum_{n=-\infty}^{\infty} \mathcal{J}_n\left(\frac{V_0}{\hbar\omega}\right) \mathrm{e}^{\mathrm{i}n\omega t} \Bigg(J_1 \sum_j \left((-1)^n \hat{c}^\dagger_{2j} \hat{c}_{2j+1} + \hat{c}^\dagger_{2j+1} \hat{c}_{2j} \right) \\ + J_2 \sum_j \left(\hat{c}^\dagger_{2j+1} \hat{c}_{2j+2} + (-1)^n \hat{c}^\dagger_{2j+2} \hat{c}_{2j+1} \right) \Bigg) + \hat{H}_A + \hat{H}_\Delta .\end{aligned} \tag{3.12}$$

Therefore, for the lowest order of the high frequency approximation, we obtain

$$\begin{aligned}\hat{H}^{(0)}_{\mathrm{D,F}} = &- J_1^{\mathrm{eff}} \sum_j (\hat{a}^\dagger_{2j} \hat{a}_{2j+1} + \mathrm{h.c.}) - J_2^{\mathrm{eff}} \sum_j (\hat{a}^\dagger_{2j+1} \hat{a}_{2j+2} + \mathrm{h.c.}) \\ &+ A \sum_j \hat{n}_j j^2 + \Delta \sum_j (-1)^j \hat{n}_j ,\end{aligned} \tag{3.13}$$

where we introduced the effective hopping amplitudes

$$J_i^{\mathrm{eff}} = J_i \mathcal{J}_0\left(\frac{V_0}{\hbar\omega}\right) \quad \text{with} \quad i \in \{1, 2\}. \tag{3.14}$$

As we can see, eq. (3.13) looks just like the expression of the static Hamilton operator of eq. (3.4). The crucial difference is that with $\hat{H}_{\mathrm{D,F}}$, we can tune the hopping amplitudes by varying the driving parameter $V_0/(\hbar\omega)$. We can even let the whole system freeze by choosing $V_0/(\hbar\omega)$ as one of the roots of $\mathcal{J}_0$. However, note that $\hat{H}_{\mathrm{D,F}}$ refers to the effective Hamiltonian describing the dynamics in the transformed system. Therefore, if we want to work with $\hat{H}_{\mathrm{D,F}}$, we need to transform all other operators as well, as

sketched in section 2.2.3. For our studies, the only relevant operators are the number operators $\hat{n}_j$. As all number operators commute with the gauge defined in eq. 3.9, the representation of the number operators in the original and the transformed system coincide. Therefore, the results from section 2.1.2 and 2.1.2 hold in both systems and can be used to numerically verify the results of the high-frequency approximation by means of two different methods:

1. We can again look at two site oscillations in the high-frequency limit for several values of $V_0/(\hbar\omega)$. If we can determine the modified frequencies of the density oscillations, we can calculate the effective hopping amplitudes using eq. (2.17).

2. By choosing $J_2 \neq 0$, we can study systems with more lattice sites. By systematically analysing the propagation of a particle in a system with $J_1 = J_2$ as a function of the driving parameters, we can also calculate the effective hopping amplitudes using the relation $\sigma \propto Jt$ derived in 2.1.2.

It is generally a good idea to have two different, independent procedures to verify a theory. In the following, we first stick with the two site oscillations and then go on with the discussion of the dynamics in a system with more sites.

3.2.1 Two Site Oscillations

We remind the reader that any T-periodic function $f(t)$ can be represented in a Fourier series by

$$f(t) = \sum_{k=-\infty}^{\infty} a_k e^{i\xi_k t}, \tag{3.15}$$

where the Fourier coefficients a_k are given by

$$a_k = \frac{1}{T}\int_0^T \mathrm{d}t\, f(t) e^{-i\xi_k t} \tag{3.16}$$

and $\xi_k = 2\pi k/T$ denotes the k-th angular frequency (for a more detailed presentation, see e.g. [16]). In the following, we will refer to the Fourier coefficients as $\mathcal{F}[f(t)](\xi_k) := a_k$.

Case 1: $\Delta = 0$

In order to calculate the frequencies of the two site density oscillations, we need to perform a Fourier transformation of the numerically calculated time evolution of $\langle \hat{n}_j \rangle$. The procedure is illustrated in fig. 3.5. In fig. 3.5 (a) and (b), the density oscillations of a particle starting at site 1 is shown for the two parameter choices $V_0/(\hbar\omega) = 0.722$ and $V_0/(\hbar\omega) = 1.686$. In order to calculate the leading frequencies of the oscillations, a Fourier transformation has to be performed as demonstrated in fig. 3.5 (c) and (d). The peak at $\xi = 0$ is caused by the zeroth Fourier coefficient, which corresponds to the overall offset of the signal and does not matter for our studies. The second peak is the most prominent one and thus indicates the leading frequency of the signal, which we will refer to as Ω_0^{eff}. There are also other frequencies in the signal whose amplitudes are suppressed compared to Ω_0^{eff}. These frequencies belong to the micromotion of the particle and are not relevant for our analysis. In order to find the dependence of Ω_0^{eff} on the ratio $V_0/(\hbar\omega)$, we repeat this procedure for several values of $V_0/(\hbar\omega)$.

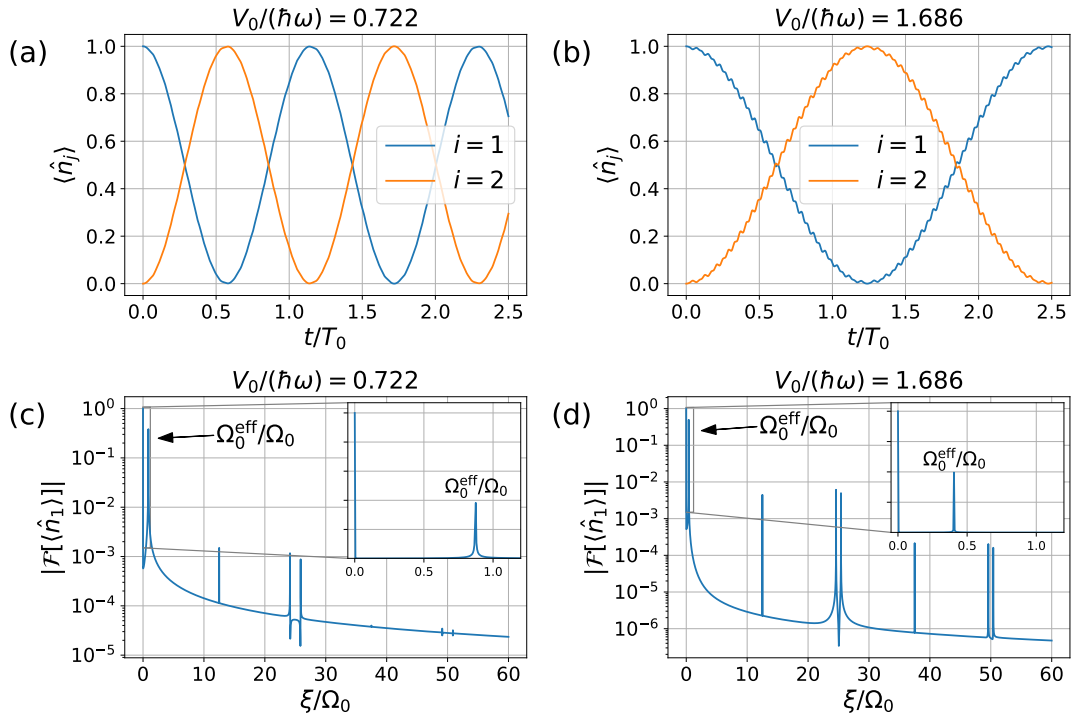

Figure 3.5: Density oscillations of a single particle with no imbalance for (a) $V_0/(\hbar\omega) = 0.722$ and (b) $V_0/(\hbar\omega) = 1.686$. Obtaining the leading frequencies of the signals by performing a Fourier transformation of $\langle \hat{n}_1 \rangle$ for (c) $V_0/(\hbar\omega) = 0.722$ and (d) $V_0/(\hbar\omega) = 1.686$. The driving frequency is given by $\hbar\omega/J_1 = 25$.

By substituting J with J_1^{eff} in eq. (2.17), we know that for $\Delta = 0$, the frequency of the two site density oscillations should be given by[1]

$$\Omega_0^{\mathrm{eff}}\left(\frac{V_0}{\hbar\omega}\right) = \left|\mathcal{J}_0\left(\frac{V_0}{\hbar\omega}\right)\right|\Omega_0, \tag{3.17}$$

where Ω_0 is the frequency of the system with no drive and no imbalance, i.e. $\Omega_0^{\mathrm{eff}}(0) = \Omega_0$. Note that this is the same Ω_0 as introduced in section 3.1.

As we can see in fig. 3.6, the numerically calculated results follow the form of eq. (3.17) predicted by the first order from the high-frequency approximation. If we choose $V_0/(\hbar\omega)$ to be equal to one of the roots of $\mathcal{J}_0$, e.g. $V_0/(\hbar\omega) \approx 2.408$, we get $\Omega_0^{\mathrm{eff}} = 0$. This means that it is not possible anymore for a particle to jump to another site, i.e. the state of the particle is frozen and does not change in time anymore. Note that this result only holds in the high frequency limit up to lowest order. If we do not choose $\hbar\omega$ large enough, we get more complicated results that cannot be analysed this easily.

Case 2: $\Delta \neq 0$

So far, we have only discussed the two site oscillations for the case $\Delta = 0$. In the following, we want to analyse how the imbalance is changing the dynamics of the system. By replacing J with J_1^{eff} on the right hand side of eq. (2.17) again, we see that the frequency of the density oscillations with imbalance has to

[1] The absolute value yields from the fact that we can only measure positive frequencies.

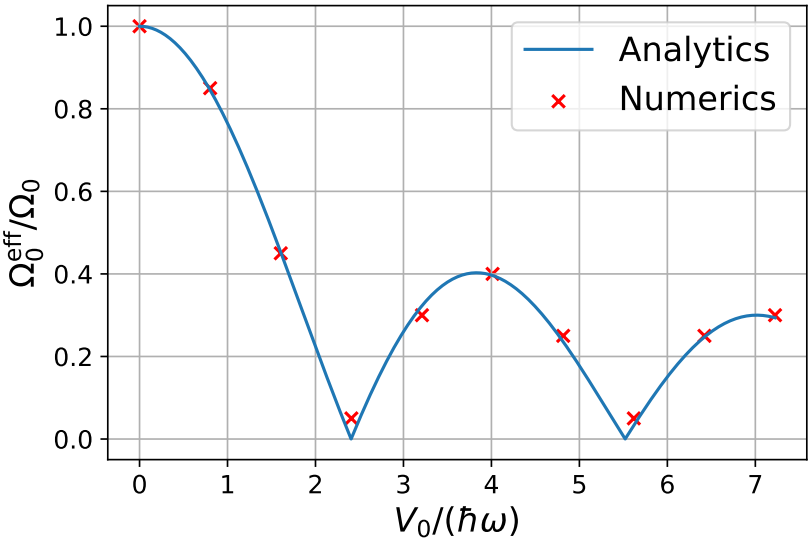

Figure 3.6: Numerically calculated dependency of the two site density oscillation frequency on the ratio of the driving parameters $V_0/(\hbar\omega)$ in comparison to the analytical result from eq. (3.17) for $\Delta = 0$. The driving frequency is $\hbar\omega/J_1 = 25$.

be modified to

$$\Omega^{\text{eff}}\left(\frac{V_0}{\hbar\omega}, \frac{\Delta}{J_1}\right) = \sqrt{\mathcal{J}_0^2\left(\frac{V_0}{\hbar\omega}\right) + \left(\frac{\Delta}{J_1}\right)^2}\,\Omega_0. \tag{3.18}$$

This expression is connected to Ω_0^{eff} introduced in the previous section by plugging in $\Delta = 0$, i.e.

$$\Omega^{\text{eff}}\left(\frac{V_0}{\hbar\omega}, 0\right) = \Omega_0^{\text{eff}}\left(\frac{V_0}{\hbar\omega}\right). \tag{3.19}$$

We notice that $\Omega^{\text{eff}}(0,0) = \Omega_0$. As we can see in fig. 3.7, the numerically calculated data for the two site oscillation frequencies match very well with our expectations from eq. (3.18). Including an imbalance generally increases the frequencies of the two site oscillations. This effect can be understood physically as well. The imbalance creates an energy offset between the two sites that scales with Δ. A particle jumping from the energetically higher site to the other receives kinetic energy. However, there is nowhere to go except for the site it just came from. The more kinetic energy the particle got, the less time it will be able to stay at the energetically lower site, thus increasing the frequency of the oscillations.

We can see from eq. (3.18), that $\Omega^{\text{eff}} \geq 2\Delta/\hbar$. This means that by including an imbalance, it is not possible anymore to dynamically localise the particle. We can observe this effect in fig. 3.7 as well. Another observation is that Ω^{eff} varies over a smaller region if the imbalance is increased. Therefore, for higher values of Δ, the effect of Floquet engineering becomes less prominent and is no efficient method to change the properties of the system anymore.

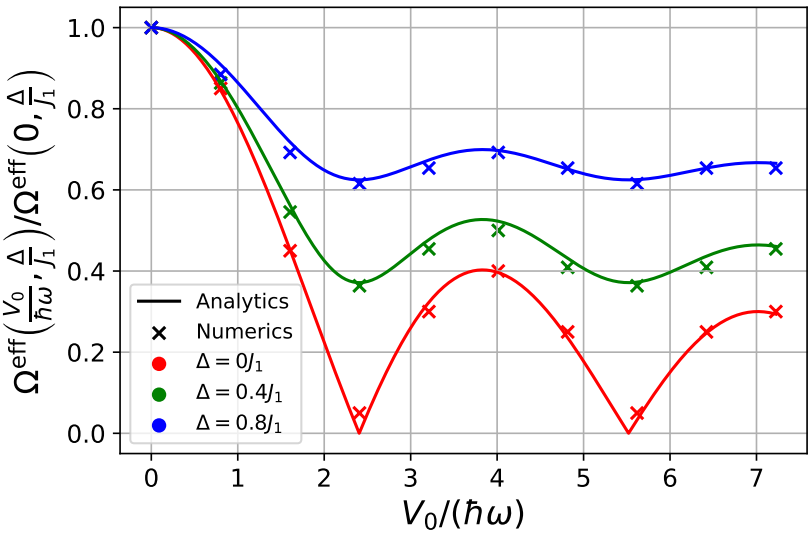

Figure 3.7: Numerically calculated dependency of the two site density oscillation frequency on the ratio of the driving parameters $V_0/(\hbar\omega)$ for several values of the imbalance Δ in comparison with the analytical results from eq. (3.18). The driving frequency is $\hbar\omega/J_1 = 25$.

3.2.2 Particle Propagation in the 1D-lattice

Now, we set $J_2 \neq 0$, allowing our particle to delocalise over the whole lattice. In this context, the harmonic oscillator introduced in eq. (3.2) can be used to limit the particles motion in the lattice. Before that, let us first have a look at the effect of the two hopping amplitudes.

In fig. 3.8 (a) we have $J_2/J_1 = 1$, yielding a random walk of the particle. As we can see, the particle starts at site 0 and delocalises over the entire lattice in a light-cone-like structure. The delocalisation process happens faster as we increase J_1 and J_2 in the same way. However, the mean position of the particle remains constant in time. In the inner of the cone, we can see an interference pattern, which is caused by particles jumping to a site from different sides with a relative phase shift.

In fig. 3.8 (b), we see the asymmetric case $J_2/J_1 = 10$. We can see that adjacent sites connected by J_2 couple to pairs. However, a particle cannot be trapped in these pairs as it can still escape by J_1. Therefore, the particle is still able to delocalise over the chain, where the time scale of this process is given by the smaller hopping amplitude (J_1 in this case). In the limit $J_2/J_1 \to \infty$, this would of course not be possible and we would get the two site model again.

In fig. 3.9, the effect of the harmonic oscillator is presented. As we can see, the harmonic oscillator limits the particle's delocalisation area in the lattice. If we increase the trapping amplitude A, the region over which the particle can delocalise becomes smaller. In fig. 3.9 (b), we can see an intensity peak at $j = 0$ and $t \approx 2.6T_0$ caused by reflections of the particle's wave function at the borders that constructively interfere in the middle.

We are now going to study the delocalisation process in a more detailed way for the symmetric case $J_1 = J_2$. The delocalisation can be quantified by looking at the standard deviation $\sigma = \sqrt{\langle j^2\rangle - \langle j\rangle^2}$ of the particle's position. We let the particle start in the middle of the lattice, i.e. $\left|\psi(t_0)\right\rangle = |0\rangle$. Recalling

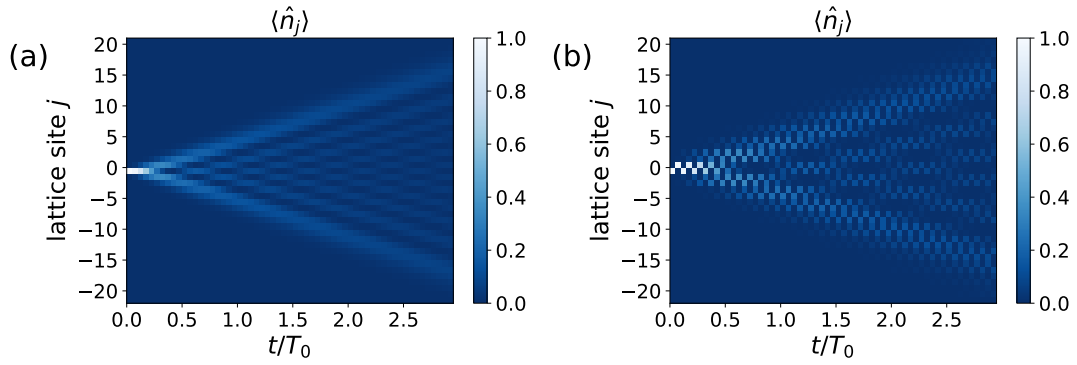

Figure 3.8: Propagation of a particle in a 1D chain without driving, trap and imbalance initially localised at site 0 for (a) the symmetric case $J_2/J_1 = 1$ and (b) the asymmetric case with $J_2/J_1 = 10$.

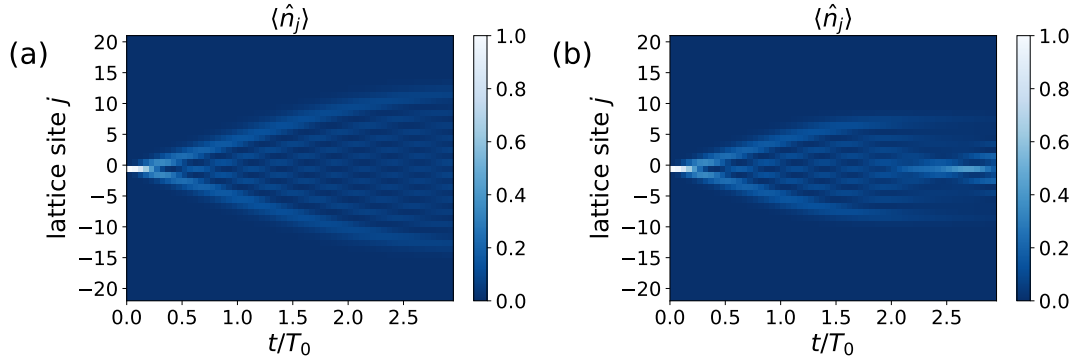

Figure 3.9: Symmetric propagation of a particle over a 1D chain with no driving and imbalance in the presence of a harmonic oscillator potential for (a) $A/J_1 = 0.02$ and (b) $A/J_1 = 0.05$.

eq. (2.20) and replacing J with J_1^{eff}, we know that

$$\sigma \propto J_1^{\text{eff}} t. \tag{3.20}$$

Therefore, by analysing the particles propagation, we can again calculate the effective hopping amplitude. In order to do so, we need to look at the time evolution of σ for several values of $V_0/(\hbar\omega)$. By fitting a linear function to our data, we calculate the scaling factor between σ and t, from which we then (up to a constant scaling factor) get the value of J^{eff}. The time evolution of σ and the corresponding line fits can be seen in fig. 3.10 (a) for selected values of $V_0/(\hbar\omega)$.

Knowing the scaling factor between σ and t for several values of the driving amplitude, we can find the dependency of J^{eff} on $V_0/(\hbar\omega)$ by making use of (3.20). The numerical results can be observed in fig. 3.10 (b). As we can see, the results again match very well with the results of the high frequency approximation (cf. eqs. (3.13) and (3.14)). Note that because $\sigma \geq 0$, we are only able to resolve the absolute value of J_1^{eff} with this procedure.

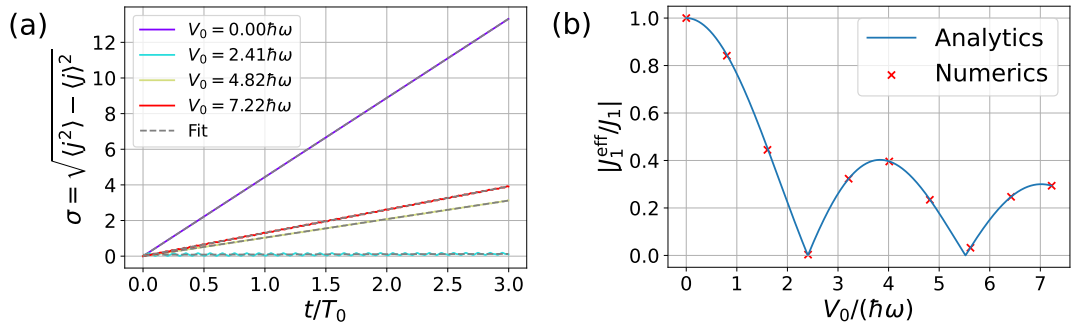

Figure 3.10: (a) Time evolution of the spatial standard deviation for various values of the ratio $V_0/(\hbar\omega)$ which by eq. (3.20) rise linearly in time. To each $V_0/(\hbar\omega)$, the evolution of σ is fitted with a line to calculate the corresponding slope which by eq. (3.20) is proportional to J_1^{eff}. (b) Resulting dependency of J_1^{eff} on $V_0/(\hbar\omega)$ in comparison with the analytical results from eq. (3.14). The parameters are $J_2/J_1 = 1, A/J_1 = \Delta/J_1 = 0, \hbar\omega/J_1 = 20$.

3.3 Summary

We studied the attributes of a Floquet driven superlattice with an additional trapping potential filled with a single particle in the limit of high-driving frequencies. We have seen that the first order of the effective Hamiltonian describing the large scale dynamics of the system resembles the Hamiltonian describing the static system with no drive, where only the hopping frequencies need to be modified by $J_i^{\text{eff}} = J_i \mathcal{J}_0\left(V_0/(\hbar\omega)\right)$. This implies that by varying the parameters of the driving, it is possible to tune the dynamics of the system with great precision. It is even possible to dynamically localise the particle by choosing the ratio $V_0/(\hbar\omega)$ to be one of the roots of $\mathcal{J}_0$.

We were then able to numerically confirm the results of the high frequency approximation firstly by looking at two site density oscillations and secondly by analysing the delocalisation process of a particle over the lattice. In the context of the density oscillations, we also studied the influence of an energetic imbalance Δ between adjacent sites. The analysis showed that the imbalance makes it impossible to localise the particle as it sets a lower limit to the density oscillation frequencies. Moreover, we saw that for large values of the imbalance, the impact of the driving becomes less significant, making the technique of Floquet engineering less effective.

CHAPTER 4

Two Particle Problem

We will now fill our system with two particles of opposite spin and allow them to interact if they are located on the same site by adding the interaction term

$$\hat{H}_U = U \sum_j \hat{n}_{j,\uparrow}\hat{n}_{j,\downarrow} \tag{4.1}$$

to our Hamiltonian. Because we later want to study bound particle pairs, we are only interested in the attractive case, i. e. $U < 0$. As we are dealing with two particles now, we need to reintroduce the sum over the spin polarisations to our model, so that the static Hamiltonian now reads

$$\begin{aligned}\hat{H}_\mathrm{S} = &-J_1 \sum_{j,\sigma}(\hat{c}^\dagger_{2j,\sigma}\hat{c}_{2j+1,\sigma} + \mathrm{h.c.}) - J_2 \sum_{j,\sigma}(\hat{c}^\dagger_{2j+1,\sigma}\hat{c}_{2j+2,\sigma} + \mathrm{h.c.}) \\ &+U \sum_j \hat{n}_{j,\uparrow}\hat{n}_{j,\downarrow} + A\sum_{j,\sigma}\hat{n}_{j,\sigma}j^2 + \Delta\sum_{j,\sigma}(-1)^j\hat{n}_{j,\sigma}.\end{aligned} \tag{4.2}$$

Again, we wish to alter the properties of the superlattice by adding the driving term

$$\hat{V}(t) = \frac{V_0}{2}\cos(\omega t)\sum_{j,\sigma}(-1)^j\hat{n}_{j,\sigma} \tag{4.3}$$

to our static system, so that the Hamilton operator of the driven system reads

$$\hat{H}(t) = \hat{H}_\mathrm{S} + \hat{V}(t). \tag{4.4}$$

We are especially interested in the strong coupling limit in which the interacting part dominates the static Hamiltonian. In this limit, the particles tend to stick together and behave like a particle pair. In order to calculate this limit analytically, one has to perform a Schrieffer-Wolff transformation. The result for the Schrieffer-Wolff transformation of the Hubbard model with a hopping and interaction term only is given in section 2.1.1. For the other terms, we use $\hat{n}_{i,\uparrow} + \hat{n}_{i,\downarrow} = 2\hat{\eta}^z_i + 1$. Up to some constant terms that can be

neglected, we get

$$\begin{aligned}\hat{H}_{\mathrm{SW}} = &-J_1^{\mathrm{p}} \sum_j (\hat{\eta}_{2j}^{+}\hat{\eta}_{2j+1}^{-} + \mathrm{h.c.}) - J_2^{\mathrm{p}} \sum_j (\hat{\eta}_{2j+1}^{+}\hat{\eta}_{2j+2}^{-} + \mathrm{h.c.}) + 2A \sum_j \hat{\eta}_j^z j^2 \\ &+2\Delta \sum_j (-1)^j \hat{\eta}_j^z + V_0 \cos(\omega t) \sum_j (-1)^j \hat{\eta}_j^z + O(\alpha_i^3),\end{aligned} \tag{4.5}$$

where we used the pair hopping amplitudes J_1^{p} and J_2^{p} defined by $J_i^{\mathrm{p}} = \frac{2J_i^2}{|U|}$ and the dimensionless variables $\alpha_i = J_i/|U| \ll 1$ with $i \in \{1, 2\}$, respectively.

4.1 Floquet-Schrieffer-Wolff Transformation

When we wish to compute the effective Hamilton operator describing our model from eq. (4.4), we need to go to the high-frequency limit again. Therefore, it does not really make sense to perform the strong coupling limit first and then calculate the high-frequency limit. Instead, the two limits need to be considered simultaneously, where the quantity $u = U/(\hbar\omega)$ remains finite. Additionally, just as in the one particle case, we want to study cases where the driving amplitude V_0 is comparably large to $\hbar\omega$. In order to compute all of these limits at the same time, one has to use an extension of the Schrieffer-Wolff transformation called Floquet-Schrieffer-Wolff transformation. The result is given by (cf. [17])

$$\begin{aligned}\hat{H}_{\mathrm{FSW}} = &-J_1^{\mathrm{p,eff}} \sum_j (\hat{\eta}_{2j}^{+}\hat{\eta}_{2j+1}^{-} + \mathrm{h.c.}) - J_2^{\mathrm{p,eff}} \sum_j (\hat{\eta}_{2j+1}^{+}\hat{\eta}_{2j+2}^{-} + \mathrm{h.c.}) \\ &+2A \sum_j \hat{\eta}_j^z j^2 + 2\Delta \sum_j (-1)^j \hat{\eta}_j^z + O(\lambda_i^3),\end{aligned} \tag{4.6}$$

where we introduced $\lambda_i = J_i/(\hbar\omega) \ll 1$ and the effective pair hopping amplitudes $J_1^{\mathrm{p,eff}}$ and $J_2^{\mathrm{p,eff}}$ defined by

$$J_i^{\mathrm{p,eff}} = \underbrace{\sum_{n=0}^{\infty} \frac{(-1)^n \mathcal{J}_n^2\left(\frac{V_0}{\hbar\omega}\right)}{1 - \frac{n}{|u|}}}_{f_u\left(\frac{V_0}{\hbar\omega}\right)} J_i^{\mathrm{p}} \quad \text{with} \quad i \in \{1, 2\}, \tag{4.7}$$

with the scaling function $f_u\left(V_0/(\hbar\omega)\right)$ normalised to $f_u(0) = 1$. Note that eq. (4.6) looks just like eq. (4.5) without a drive, i. e. the strong coupling limit of the static Hamiltonian given in eq. (4.2), where we only need to replace the pair hopping amplitudes J_i^{p} with the effective pair hopping amplitudes $J_i^{\mathrm{p,eff}}$ depending on the parameters of the driving. This is very similar to what we obtained in eqs. (3.13) and (3.14) for a single particle. However, In the one particle case, the scaling function between the effective amplitudes J_i^{eff} and the original amplitudes J_i is given by $\mathcal{J}_0\left(V_0/\hbar\omega\right)$ (cf. eq. (3.14)). Now, we have to deal with the more complicated function $f_u\left(V_0/(\hbar\omega)\right)$ instead. A plot of this function can be seen in fig. 4.1 for several values of $|u|$. Looking at eq. (4.7), we see that the new scaling function becomes divergent if $|u| \in \mathbb{N}$. For this choice of $|u|$, the driving frequency matches the band gap energy created by U, making it possible to excite particles to higher Bloch bands. We refer to this as the resonant case. In our numerics, we do not want to deal with divergent terms, which is why we try to avoid the resonance

and choose $|u| \notin \mathbb{N}$. For $|u| \to \infty$ and $|u| \notin \mathbb{N}$, we can see that $f_u\left(V_0/(\hbar\omega)\right)$ converges to

$$f_{|u|\to\infty}\left(\frac{V_0}{\hbar\omega}\right) = \sum_{n=0}^{\infty}(-1)^n \mathcal{J}_n^2\left(\frac{V_0}{\hbar\omega}\right). \tag{4.8}$$

This convergence can also be observed in fig. 4.1. For $|u| = 1.2$ and $|u| = 4.3$, we do not see any convergence yet, but the other functions match over an extended interval already.

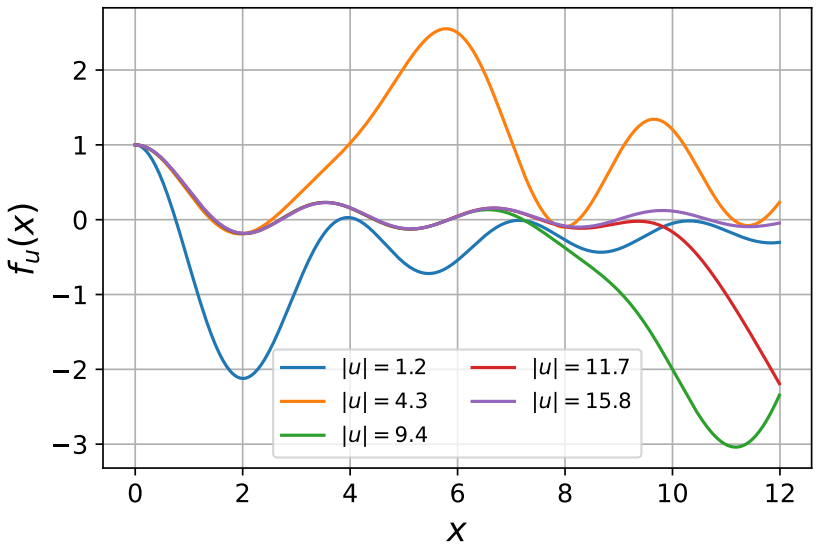

Figure 4.1: Plot of the scaling function $f_u(x)$ appearing in eq. (4.7) for several values of the ratio $|u| = |U|/(\hbar\omega)$ of the interaction amplitude U and the energy $\hbar\omega$ associated with the driving frequency.

In the following, we would like to verify eq. (4.7) numerically. In order to do so, we pay attention to the two site pair density oscillations and the propagation of the particle pair over the 1D chain again. Let us start with the two site oscillations.

4.1.1 Two Site Pair Oscillations

For the particle pair model with kinetic part only, we can calculate the two site oscillation frequency Ω_0^{p} using eq. (2.17) by replacing the single particle hopping amplitude J_1 with the pair hopping amplitude J_1^{p} and setting $\Delta = 0$. We get $\Omega_0^{\mathrm{p}} = 2J_1^{\mathrm{p}}/\hbar = 4J_1^2/\hbar|U|$, corresponding to the period $T_0^{\mathrm{p}} = \pi\hbar/J_1^{\mathrm{p}} = \pi\hbar|U|/\left(2J_1^2\right)$, which we are going to use as a reference time.

Case 1: $\Delta = 0$

First, we discuss the case with no imbalance again. We proceed in the same way as we did for the single particle case in section 3.2.1. The two upper plots of fig. 4.2 show the two site density oscillation of the particle pair for (a) $V_0/(\hbar\omega) = 2.0$ and (b) $V_0/(\hbar\omega) = 5.5$. In (c) and (d), we can see the corresponding frequency spectra calculated with a Fourier tranformation of $\langle \hat{n}_{1,\uparrow}\hat{n}_{1,\downarrow}\rangle$. The leading frequency $\Omega_0^{\mathrm{p,eff}}$ again is the one with the most prominent peak in the spectrum, apart from the one at $\xi = 0$.

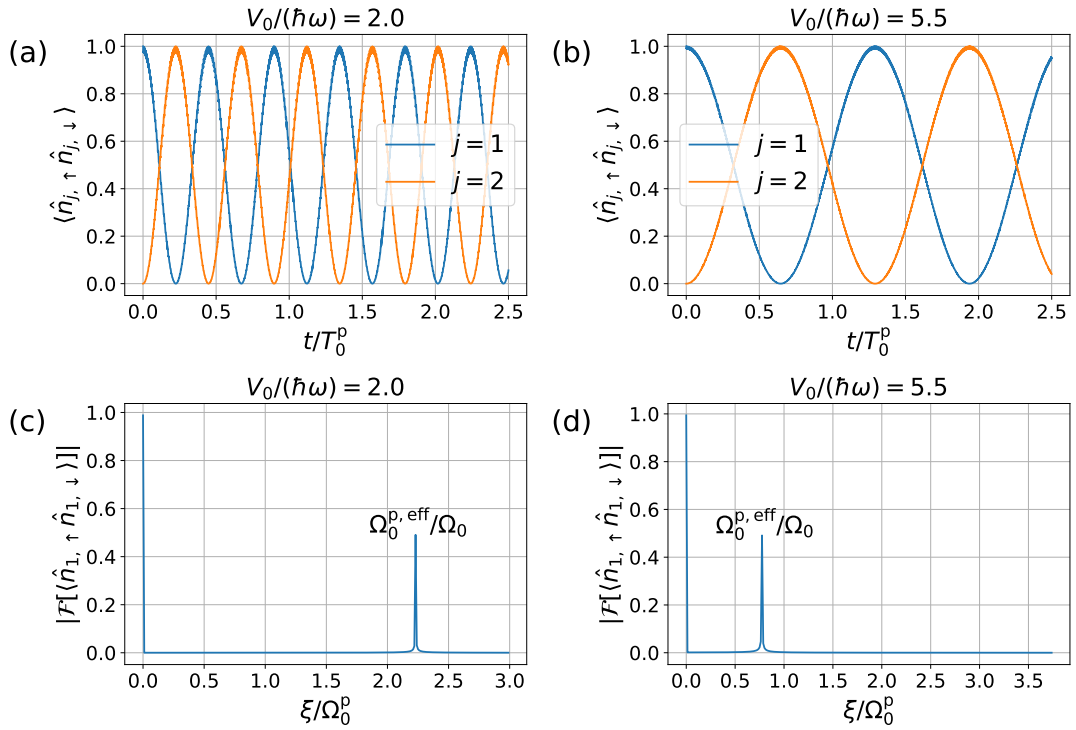

Figure 4.2: Density oscillations of the particle pair for (a) $V_0/(\hbar\omega) = 2.0$ and (b) $V_0/(\hbar\omega) = 5.5$. Obtaining the leading frequencies of the signals by performing a Fourier transform of $\langle \hat{n}_{\uparrow,1} \hat{n}_{\downarrow,1} \rangle$ for (c) $V_0/(\hbar\omega) = 2.0$ and (d) $V_0/(\hbar\omega) = 5.5$. The parameters are $|u| = 1.2, \hbar\omega/J_1 = 50$.

By replacing J with $J_1^{\mathrm{p,eff}}$ in eq. (2.17) and setting $\Delta = 0$, we would expect the frequency of the two site density oscillations of the particle pair to behave like[1]

$$\Omega_0^{\mathrm{p,eff}}\left(\frac{V_0}{\hbar\omega}\right) = \left| f_u\left(\frac{V_0}{\hbar\omega}\right)\right| \Omega_0^{\mathrm{p}}. \tag{4.9}$$

Note that for no driving, we get $\Omega_0^{\mathrm{p,eff}}(0) = \Omega_0^{\mathrm{p}}$. Calculating $\Omega_0^{\mathrm{p,eff}}$ for several values of $V_0/\hbar\omega$ with the procedure demonstrated in fig. 4.2, we arrive at the results shown in fig. 4.3. We can see that the numerically calculated results agree very well with eq. (4.9). In our calculations, we chose $|u| = 1.2$. We can see that for this choice, $\Omega_0^{\mathrm{p,eff}}$ vanishes for $V_0/(\hbar\omega) \approx 0.754$ and around $V_0/(\hbar\omega) \approx 4$. Therefore, it is possible to dynamically localise the particle pair as well. However, the freezing points of the two particle system do not coincide with those of the single particle system and depend on the choice of $|u|$. Thus, it is possible to choose the driving parameters in a way so that single particles freeze and pairs do not, and vice versa. Another interesting effect is that in contrast to the single particle case, we can find parameters of the driving so that $\Omega_0^{\mathrm{p,eff}} > \Omega_0^{\mathrm{p}}$.

[1] Again, the absolute value yields from the fact that we cannot measure negative frequencies.

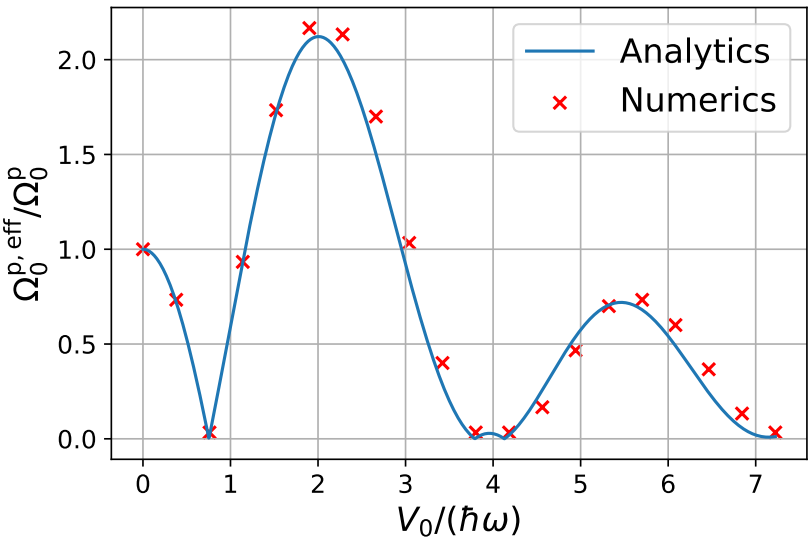

Figure 4.3: Numerically calculated dependency of the two site density oscillation frequency of the particle pair on the ratio of the driving parameters $V_0/(\hbar\omega)$ with no imbalance in comparison to the analytical result from eq. (4.9). The parameters are $|u| = 1.2, \hbar\omega/J_1 = 50$.

Case 2: $\Delta \neq 0$

We now go on we studying the effect of the imbalance again. Replacing Δ with 2Δ due to the additional factor of 2 in front of the staggered term in eq. (4.5) and substituting $J_1^{p,\mathrm{eff}}$ for J in eq. (2.17), we get

$$\Omega^{p,\mathrm{eff}}\left(\frac{V_0}{\hbar\omega}, \frac{\Delta}{J_1^p}\right) = \sqrt{f_u^2\left(\frac{V_0}{\hbar\omega}\right) + \left(\frac{2\Delta}{J_1^p}\right)^2}\,\Omega_0^p. \tag{4.10}$$

Analogously to the single particle case, the connection between $\Omega^{p,\mathrm{eff}}$ and $\Omega_0^{p,\mathrm{eff}}$ introduced in section 4.1.1 is given by

$$\Omega^{p,\mathrm{eff}}\left(\frac{V_0}{\hbar\omega}, 0\right) = \Omega_0^{p,\mathrm{eff}}\left(\frac{V_0}{\hbar\omega}\right). \tag{4.11}$$

Also, we find $\Omega^{p,\mathrm{eff}}(0,0) = \Omega_0^p$. A comparison between eq. (4.10) and the numerical results for $|u| = 1.2$ is visualised in fig. 4.4. Just as in the single particle case, we see that the imbalance sets a lower limit to the oscillation frequencies given by $2\Delta/\hbar$, preventing the system from freezing. Moreover, the influence of the driving is suppressed if the imbalance is increased, making the concept of Floquet engineering less effective for large values of Δ

4.1.2 Pair Propagation in the 1D lattice

Knowing about the two site oscillations of the pair density, we now go on analysing the time evolution of the delocalisation of a particle pair over a 1D lattice with symmetric hopping amplitudes (i.e. $J_1 = J_2$) as

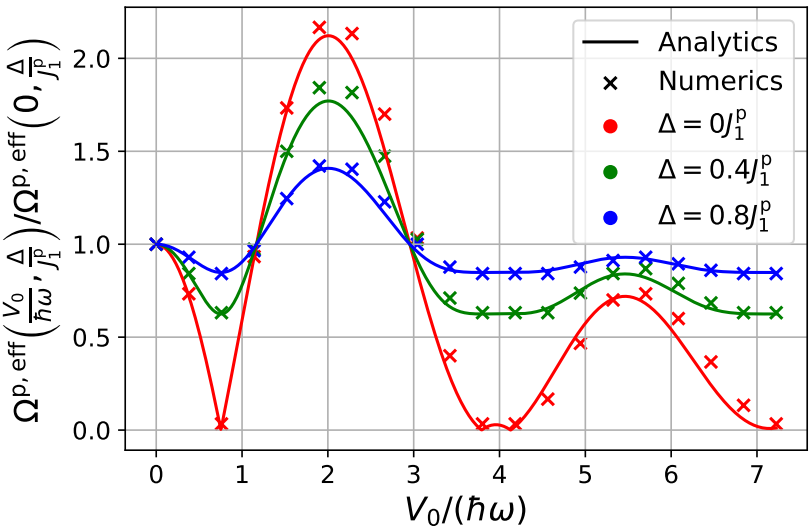

Figure 4.4: Numerically calculated dependency of the two site density oscillation frequency of the particle pair on the ratio of the driving parameters $V_0/(\hbar\omega)$ for several values of the imbalance in comparison with the analytical results from eq. (4.10). The parameters are $|u| = 1.2, \hbar\omega/J_1 = 50$.

a function of the driving. By replacing J with $J_1^{\mathrm{p,eff}}$ in eq. (2.20), we find the linear relation

$$\sigma \propto J_1^{\mathrm{p,eff}} t \tag{4.12}$$

between the spatial standard deviation of the particle pair σ and the effective hopping amplitude $J_1^{\mathrm{p,eff}}$. We can use the time evolution of the operator

$$\hat{N}_{\mathrm{D}} = \sum_j \hat{n}_{j,\uparrow}\hat{n}_{j,\downarrow} \tag{4.13}$$

that projects on the subspace of states where the two particles are located on the same site to evaluate whether the particles stay bound as a pair. In fig. 4.5 (a), we see the time evolution for the expectation value of the pair density operator $\hat{n}_{j,\uparrow}\hat{n}_{j,\downarrow}$. We recognise the light-cone like shape that we observed in the one particle model (see fig. 3.8). In fig. 4.5 (b), the corresponding time evolution of $\langle\hat{N}_{\mathrm{D}}\rangle$ is visualised to verify the stability of the strong coupling limit. At worst, the probability to find the two particles on different sites is 0.40 %. In the limit of $U \to \infty$, this probability identically vanishes. However, as this limit cannot be realised experimentally, the current parameter choice is suitable[2].

Analogously to the one particle case, we can now analyse the time evolution of the spatial standard deviation to calculate the dependency of the effective hopping amplitude on the driving parameters. The results can be seen in fig. 4.6. In fig. 4.6 (a), we see the linear time evolution of σ for specific values of $V_0/(\hbar\omega)$. To each curve, we fit a straight line in order to calculate the scaling factor between σ and t, which by eq. (4.12) is proportional to the effective pair hopping amplitude. Repeating this procedure

[2] Note that in fig. 4.5, we calculated the evolution of $\langle\hat{n}_{j,\uparrow}\hat{n}_{j,\downarrow}\rangle$ and $\langle\hat{N}_{\mathrm{D}}\rangle$ for 13 sites over a time span of $0 \leq t \leq 0.8T_0$ in order to resolve the light cone structure. In order to keep the runtime of the program down, it will be sufficient to consider 5 sites and a time span of $0 \leq t \leq 0.16T$ for the next calculations.

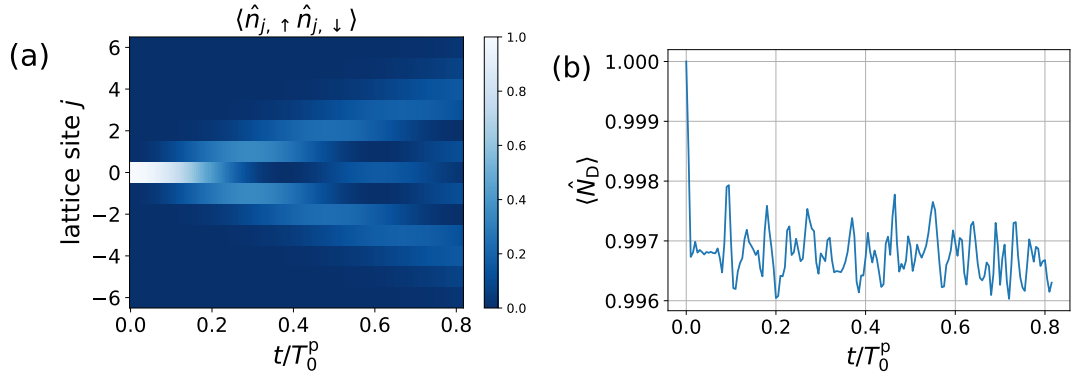

Figure 4.5: (a) Propagation of the effective particle pair over the 1D chain without driving, particle trap and imbalance and (b) verifying the stability of the strong coupling limit by looking at the probability to find the particles on the same site given by $\langle \hat{N}_D \rangle$ defined in eq. (4.13). The ratio of interaction amplitude and energy associated with the driving frequency is $|u| = 1.25$.

for several values of the driving parameters, we can resolve the dependency of the effective hopping amplitude on $V_0/(\hbar\omega)$ shown in fig. 4.6 (b). As we can see, the numerically calculated results agree very well with eq. (4.7).

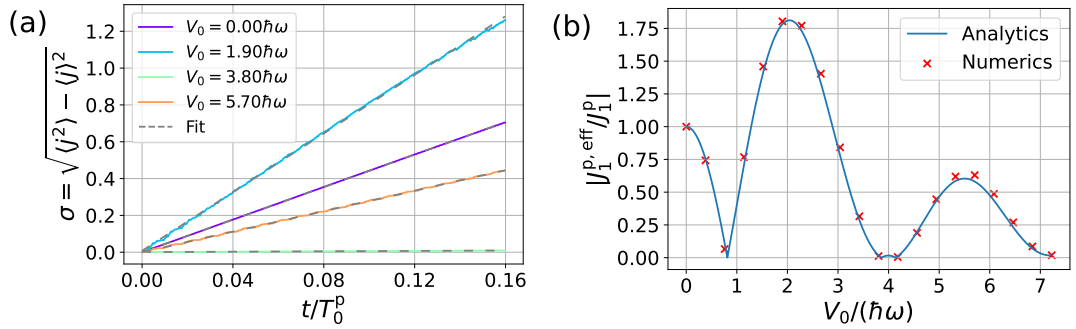

Figure 4.6: (a) Time evolution of the spatial standard deviation of the particle pair for various values of the ratio $V_0/(\hbar\omega)$ which by eq. (4.12) rise linearly in time. To each $V_0/(\hbar\omega)$, the evolution is fitted with a line to calculate the corresponding slope which by eq. (4.12) is proportional to the effective hopping amplitude. (b) Resulting dependency of the effective hopping amplituder, on $V_0/(\hbar\omega)$ in comparison with the analytical results from eq. (4.7). The parameters are $|u| = 1.25, J_2/J_1 = 1, A/J_1 = \Delta/J_1 = 0, \hbar\omega/J_1 = 40$.

4.2 Summary

We looked at the properties of a Floquet driven superlattice with an additional trapping potential filled with two on-site interacting particles. Due to the interaction, the solution of this model does not factorise into two one particle solutions, complicating the problem a little more. First of all, we had to find a simplified expression of the effective Hamiltonian for the combined limit of strong coupling and high driving frequencies. Calculations show that in the combination of these two limits, the effective Hamiltonian resembles that of the model with no drive with effective hopping amplitudes. The effective

hopping amplitudes depend on the driving parameters and the interaction amplitude in a complicated fashion. By making use of numerical methods, we were able to confirm this dependency.

Analogously to the one particle case, we looked firstly at the two site pair density oscillations and secondly at the propagation of a particle pair over the 1D chain. We observed that for specific values of the driving parameters that are depending on the interaction amplitude, it is possible to freeze the dynamics of the system.

In the context of the two site oscillations, we saw that including an energetic imbalance between the two sites sets a lower limit to the frequency, preventing the system from freezing. Moreover, the analysis showed that for large imbalances, the effect of the driving is suppressed.

CHAPTER 5

Conclusion

The concept of Floquet engineering has successfully been applied to a 1D superlattice to tune its transport parameters. We saw that in general, by applying a time periodic drive to a quantum mechanical system, the stroboscopic time evolution of the driven system is described by a time independent effective Hamilton operator that can be very different from the original Hamiltonian.

First, we investigated the superlattice filled with one particle. We saw that in the limit of high driving frequencies ω, the effective Hamiltonian up to zeroth order in ω^{-1} resembles the static Hamiltonian with effective hopping amplitudes that depend on the parameters of the driving. We were able to numerically verify this result by analysing the frequencies of two site density oscillations, and by studying the delocalisation process of a particle in the lattice. An interesting effect is that for certain choices of the driving parameters, it is possible to dynamically localise the particle. In the context of the two site oscillations, we saw that by introducing an energetic imbalance between the sites, the influence of the drive is suppressed, preventing the system from freezing.

Afterwards, we added a second particle with opposite spin to the system and allowed the two particles to attractively interact when located on the same site. We then applied the same drive to the system as we did in the single particle case. Calculations show that in the limit of strong (attractive) on-site interactions and high driving frequencies, the effective Hamiltonian takes the form of a Hamilton operator describing the dynamics of a particle pair with effective hopping amplitudes depending on the parameters of the driving and the interaction amplitude in a complicated way. We were able to numerically confirm this dependency by using the methods of the one particle problem. Furthermore, we saw that the imbalance has the same effects on the two site oscillations of the particle pair as on those of the single particle.

The two most significant differences between the one and two particle case is that firstly, the values of the driving parameters for which the system freezes do not coincide and are dependent on the interaction amplitude in the two particle case. Secondly, for the two particle system, it is possible to increase the hopping amplitudes by adapting the driving parameters. For a single particle, this cannot be done.

In spite of the detailed discussion, there is still some work left that could be done in the future. E.g., the influence of the staggered potential on the delocalisation process of the particle and the pair particle has not been discussed yet. Furthermore, the effect of the particle trap on the delocalisation of the particle has to be analysed with more care. Higher orders of the high-frequency approximation could be considered to get a better understanding of the driven system for lower frequencies of the driving. Moreover, the dynamics of a superlattice filled with with more than two particles can be investigated. Presumably, this is the most sophisticated task.

Bibliography

[1] A. Eckardt, *Colloquium: Atomic quantum gases in periodically driven optical lattices*, Rev. Mod. Phys. **89** (1 2017) 011004, URL: https://link.aps.org/doi/10.1103/RevModPhys.89.011004 (cit. on p. 1).

[2] H. Lignier et al., *Dynamical Control of Matter-Wave Tunneling in Periodic Potentials*, Phys. Rev. Lett. **99** (22 2007) 220403, URL: https://link.aps.org/doi/10.1103/PhysRevLett.99.220403 (cit. on p. 1).

[3] E. Kierig, U. Schnorrberger, A. Schietinger, J. Tomkovic and M. K. Oberthaler, *Single-Particle Tunneling in Strongly Driven Double-Well Potentials*, Phys. Rev. Lett. **100** (19 2008) 190405, URL: https://link.aps.org/doi/10.1103/PhysRevLett.100.190405 (cit. on p. 1).

[4] C. E. Creffield, F. Sols, D. Ciampini, O. Morsch and E. Arimondo, *Expansion of matter waves in static and driven periodic potentials*, Phys. Rev. A **82** (3 2010) 035601, URL: https://link.aps.org/doi/10.1103/PhysRevA.82.035601 (cit. on p. 1).

[5] A. Eckardt et al., *Exploring dynamic localization with a Bose-Einstein condensate*, Physical Review A **79** (2009) 013611 (cit. on p. 1).

[6] C. Sias et al., *Observation of Photon-Assisted Tunneling in Optical Lattices*, Phys. Rev. Lett. **100** (4 2008) 040404, URL: https://link.aps.org/doi/10.1103/PhysRevLett.100.040404 (cit. on p. 1).

[7] A. Zenesini, H. Lignier, D. Ciampini, O. Morsch and E. Arimondo, *Coherent Control of Dressed Matter Waves*, Phys. Rev. Lett. **102** (10 2009) 100403, URL: https://link.aps.org/doi/10.1103/PhysRevLett.102.100403 (cit. on p. 1).

[8] N. Gemelke, E. Sarajlic, Y. Bidel, S. Hong and S. Chu, *Parametric Amplification of Matter Waves in Periodically Translated Optical Lattices*, Phys. Rev. Lett. **95** (17 2005) 170404, URL: https://link.aps.org/doi/10.1103/PhysRevLett.95.170404 (cit. on p. 1).

[9] M. Aidelsburger et al., *Experimental Realization of Strong Effective Magnetic Fields in an Optical Lattice*, Phys. Rev. Lett. **107** (25 2011) 255301, URL: https://link.aps.org/doi/10.1103/PhysRevLett.107.255301 (cit. on p. 1).

[10] J. Hubbard, *Electron correlations in narrow energy bands*, Proceedings of the Royal Society of London. Series A. Mathematical and Physical Sciences **276** (1963) 238, URL: https://royalsocietypublishing.org/doi/10.1098/rspa.1963.0204 (cit. on p. 2).

[11] F. H. Essler, H. Frahm, F. Göhmann, A. Klümper and V. E. Korepin, *The one-dimensional Hubbard model*, Cambridge University Press, 2005 (cit. on pp. 3, 4).

[12] G. Floquet, *Sur les équations différentielles linéaires à coefficients périodiques*, fr, Annales scientifiques de l'École Normale Supérieure **2e série, 12** (1883) 47, URL: http://www.numdam.org/articles/10.24033/asens.220/ (cit. on p. 6).

[13] A. Eckardt and E. Anisimovas, *High-frequency approximation for periodically driven quantum systems from a Floquet-space perspective*, New Journal of Physics **17** (2015) 093039, URL: https://doi.org/10.1088/1367-2630/17/9/093039 (cit. on pp. 6, 9).

[14] M. Holthaus, *Floquet engineering with quasienergy bands of periodically driven optical lattices*, Journal of Physics B: Atomic, Molecular and Optical Physics **49** (2015) 013001, URL: https://doi.org/10.1088/0953-4075/49/1/013001 (cit. on p. 6).

[15] D. W. Lozier, *NIST digital library of mathematical functions*, Annals of Mathematics and Artificial Intelligence **38** (2003) 105, URL: https://dlmf.nist.gov (cit. on p. 15).

[16] B. Boashash, *Time-frequency signal analysis and processing: a comprehensive reference*, Academic press, 2015 (cit. on p. 17).

[17] F. Hübner, "Bound Pairs Scattering off a Floquet Driven Impurity", Masterarbeit, 2021 (cit. on pp. 24, 38).

APPENDIX A

Pair Operators

In section 2.1.1, we mentioned that the pair "creation" and "annihilation" operators defined in eq. (2.8) are part of a spin-$\frac{1}{2}$-algebra. We are now going to clarify what this is supposed to mean. The operators $\hat{\eta}^{\pm}$ do not obey the fermionic anticommutation relation from eq. (2.2), but follow the relations

$$\begin{aligned} \{\hat{\eta}_i^{\pm}, \hat{\eta}_j^{\pm}\} &= 2\hat{\eta}_i^{\pm}\hat{\eta}_j^{\pm} \\ \{\hat{\eta}_i^{+}, \hat{\eta}_j^{-}\} &= 2\hat{\eta}_i^{+}\hat{\eta}_j^{-} - 2\delta_{ij}\hat{\eta}_i^{z}. \end{aligned} \tag{A.1}$$

From these relations, we can calculate the corresponding commutations relations using the formula

$$[\hat{A}, \hat{B}] = 2\hat{A}\hat{B} - \{\hat{A}, \hat{B}\}. \tag{A.2}$$

We arrive at the results

$$\begin{aligned} [\hat{\eta}_i^{\pm}, \hat{\eta}_j^{\mp}] &= 0 \\ [\hat{\eta}_i^{+}, \hat{\eta}_j^{-}] &= 2\delta_{ij}\hat{\eta}_i^{z}. \end{aligned} \tag{A.3}$$

We now introduce the two operators

$$\hat{\eta}_i^{x} = \frac{1}{2}(\hat{\eta}_i^{+} + \hat{\eta}_i^{-}) \tag{A.4}$$

$$\hat{\eta}_i^{y} = -\frac{\mathrm{i}}{2}(\hat{\eta}_i^{+} - \hat{\eta}_i^{-}) \tag{A.5}$$

that, together with the operator $\hat{\eta}_i^{z}$, obey the commutation relations

$$[\hat{\eta}_i^{\alpha}, \hat{\eta}_j^{\beta}] = \mathrm{i}\epsilon^{\alpha\beta\gamma}\delta_{ij}\hat{\eta}_i^{\gamma}, \tag{A.6}$$

where $\epsilon^{\alpha\beta\gamma}$ is the totally antisymmetric Levi-Civita tensor and $\alpha, \beta, \gamma \in \{x, y, z\}$. Eq. (A.6) resembles the commutation relations of the components of the angular momentum operator $\hat{\boldsymbol{J}}$. Therefore, we can identify the operators $\hat{\eta}_i^{x}, \hat{\eta}_j^{y}, \hat{\eta}_k^{z}$ with the compontents $\hat{J}_i^{x}, \hat{J}_j^{y}$ and $\hat{J}_k^{z}$. Moreover, we find the commutation relations

$$[\hat{\eta}_i^{z}, \hat{\eta}_j^{\pm}] = \pm\delta_{ij}\hat{\eta}_i^{\pm}, \tag{A.7}$$

which is equivalent to the commutation relations of the operator $\hat{J}_i^z$ with the ladder operators $\hat{J}_i^{\pm} = \hat{J}_i^x \pm \mathrm{i}\hat{J}_i^y$. Because we are dealing with fermions, we know that $(\hat{\eta}_i^+)^2 = (\hat{\eta}_i^-)^2 = 0$, which is characteristic for spin-$\frac{1}{2}$-algebras. Hence, we can associate the pair "creation" and "annihilation" operators $\hat{\eta}_i^{\pm}$ with the ladder operators $\hat{S}_i^{\pm}$ of a spin-$\frac{1}{2}$-algebra. The Casimir operator $\hat{\boldsymbol{\eta}}^2$ of the algebra spanned by $\{\hat{\eta}_j^x, \hat{\eta}_k^y, \hat{\eta}_l^z\}$ is then given by

$$\hat{\boldsymbol{\eta}}^2 = \sum_{\alpha \in \{x,y,z\}} (\hat{\eta}_i^{\alpha})^2. \tag{A.8}$$

APPENDIX B

Spectral Theorem for Unitary Operators

In this chapter, we prove that for every unitary operator, there exists an orthonormal eigenbasis. In order to show this, let us first have a look at an operator $\hat{A}$ that is invertible, i.e. $\det\left(\hat{A}\right) \neq 0$. Let $|n\rangle$ be an eigenvalue of $\hat{A}$, i.e.

$$\hat{A}\,|n\rangle = a_n\,|n\rangle\,. \tag{B.1}$$

By letting the inverse operator $\hat{A}^{-1}$ act on both sides of this equation and dividing by a_n, we get

$$\hat{A}^{-1}\,|n\rangle = \frac{1}{a_n}\,|n\rangle \tag{B.2}$$

for $a_n \neq 0$. This means that the eigenstates $|n\rangle$ of $\hat{A}$ with eigenvalue a_n are eigenstates of the inverse operator $\hat{A}^{-1}$ as well with eigenvalues a_n^{-1}. Let $|n\rangle$ and $|m\rangle$ be two eigenstates of the unitary operator $\hat{B}$ with different eigenvalues b_n and b_m. Then, we have

$$\hat{B}^{\dagger}\,|n\rangle = \hat{B}^{-1}\,|n\rangle = \frac{1}{b_n}\,|n\rangle\,. \tag{B.3}$$

By taking the adjoint of this equation, we see that

$$\langle n|\,\hat{B} = \langle n|\,\frac{1}{b_n^*}. \tag{B.4}$$

This means that for the matrix element $\langle n|\,\hat{B}\,|m\rangle$, we find

$$\langle n|\,\hat{B}\,|m\rangle = (b_n^{-1})^*\,\langle n|m\rangle = b_m\,\langle n|m\rangle\,. \tag{B.5}$$

Using the fact that the eigenvalues of a unitary operator have absolute value 1, we find that $(b_n^{-1})^* = b_n$. By substracting the right side of eq. (B.5) from the left side, we obtain

$$\underbrace{(b_n - b_m)}_{\neq 0}\,\langle n|m\rangle = 0. \tag{B.6}$$

This implies that for $b_n \neq b_m$, we have $\langle n|m\rangle = 0$. For $b_n = b_m$ but linearly independent $|n\rangle, |m\rangle$, it is always possible to construct the states $\left|n'\right\rangle, \left|m'\right\rangle$ as a linear combination of $|n\rangle, |m\rangle$ so that $\left\langle n'\middle|m'\right\rangle = 0$. Therefore, for a unitary operator $\hat{B}$, there exists an orthonormal eigenbasis.

APPENDIX C

High-Frequency Expansion

When calculating the high frequency expansion in section 3.2, we need to calculate the expression

$$\hat{H}_{\mathrm{D}}(t) = \mathrm{e}^{\mathrm{i}\lambda(t)\hat{A}}\hat{H}_{\mathrm{S}}\mathrm{e}^{-\mathrm{i}\lambda(t)\hat{A}}, \tag{C.1}$$

with $\lambda(t) = V_0/(2\hbar\omega)\sin(\omega t)$ and $\hat{A} = \sum_j (-1)^j \hat{n}_j$. In the following, we suppress the argument of λ for readability. We know that

$$[\hat{A}, \hat{n}_j] = 0. \tag{C.2}$$

Therefore, eq. (C.1) simplifies to

$$\hat{H}_{\mathrm{D}}(t) = \mathrm{e}^{\mathrm{i}\lambda\hat{A}}\hat{H}_J\mathrm{e}^{-\mathrm{i}\lambda\hat{A}} + \hat{H}_A + \hat{H}_\Delta. \tag{C.3}$$

In the first part on the right of this equation, we come across the four terms

$$\hat{O}_{1,j}(\lambda) = \mathrm{e}^{\mathrm{i}\lambda\hat{A}}\hat{c}^\dagger_{2j}\hat{c}_{2j+1}\mathrm{e}^{-\mathrm{i}\lambda\hat{A}} \tag{C.4}$$

$$\hat{O}_{2,j}(\lambda) = \mathrm{e}^{\mathrm{i}\lambda\hat{A}}\hat{c}^\dagger_{2j+1}\hat{c}_{2j}\mathrm{e}^{-\mathrm{i}\lambda\hat{A}} \tag{C.5}$$

$$\hat{O}_{3,j}(\lambda) = \mathrm{e}^{\mathrm{i}\lambda\hat{A}}\hat{c}^\dagger_{2j+1}\hat{c}_{2j+2}\mathrm{e}^{-\mathrm{i}\lambda\hat{A}} \tag{C.6}$$

$$\hat{O}_{4,j}(\lambda) = \mathrm{e}^{\mathrm{i}\lambda\hat{A}}\hat{c}^\dagger_{2j+2}\hat{c}_{2j+1}\mathrm{e}^{-\mathrm{i}\lambda\hat{A}}. \tag{C.7}$$

We will now present a method taken from [17] to calculate these expressions, using $\hat{O}_{1,j}(\lambda)$ as an example. Deriving $\hat{O}_{1,j}(\lambda)$ with respect to λ yields

$$\frac{\mathrm{d}}{\mathrm{d}\lambda}\hat{O}_{1,j}(\lambda) = \mathrm{i}\mathrm{e}^{\mathrm{i}\lambda\hat{A}}[\hat{A}, \hat{c}^\dagger_{2j}\hat{c}_{2j+1}]\mathrm{e}^{-\mathrm{i}\lambda\hat{A}}. \tag{C.8}$$

Making use of the commutator relation

$$[\hat{A}, \hat{c}^\dagger_{2j}\hat{c}_{2j+1}] = 2\hat{c}^\dagger_{2j}\hat{c}_{2j+1}, \tag{C.9}$$

we end up with

$$\frac{\mathrm{d}}{\mathrm{d}\lambda}\hat{O}_{1,j}(\lambda) = 2\mathrm{i}\hat{O}_{1,j}(\lambda). \tag{C.10}$$

This differential equation can easily be solved, using the initial condition $\hat{O}_{1,j}(0) = \hat{c}^\dagger_{2j}\hat{c}_{2j+1}$ from eq. (C.4). We obtain

$$\hat{O}_{1,j}(\lambda) = \hat{c}^\dagger_{2j}\hat{c}_{2j+1}\mathrm{e}^{2\mathrm{i}\lambda}. \tag{C.11}$$

Analogously, using the commutation relations

$$[\hat{A}, \hat{c}^\dagger_{2j+1}\hat{c}_{2j}] = -2\hat{c}^\dagger_{2j+1}\hat{c}_{2j} \tag{C.12}$$
$$[\hat{A}, \hat{c}^\dagger_{2j+1}\hat{c}_{2j+2}] = -2\hat{c}^\dagger_{2j+1}\hat{c}_{2j+2} \tag{C.13}$$
$$[\hat{A}, \hat{c}^\dagger_{2j+2}\hat{c}_{2j+1}] = 2\hat{c}^\dagger_{2j+2}\hat{c}_{2j+1}, \tag{C.14}$$
$$\tag{C.15}$$

we find the expressions

$$\hat{O}_{2,j}(\lambda) = \hat{c}^\dagger_{2j+1}\hat{c}_{2j}\mathrm{e}^{-2\mathrm{i}\lambda} \tag{C.16}$$
$$\hat{O}_{3,j}(\lambda) = \hat{c}^\dagger_{2j+1}\hat{c}_{2j+2}\mathrm{e}^{-2\mathrm{i}\lambda} \tag{C.17}$$
$$\hat{O}_{4,j}(\lambda) = \hat{c}^\dagger_{2j+2}\hat{c}_{2j+1}\mathrm{e}^{2\mathrm{i}\lambda} \tag{C.18}$$

for the remaining terms. Plugging all into eq. (C.3), we obtain

$$\begin{aligned}\hat{H}_\mathrm{D}(t) &= -\mathrm{e}^{\mathrm{i}\lambda\hat{A}}\left(J_1\sum_j\left(\hat{c}^\dagger_{2j}\hat{c}_{2j+1} + \hat{c}^\dagger_{2j+1}\hat{c}_{2j}\right) + J_2\sum_j\left(\hat{c}^\dagger_{2j+1}\hat{c}_{2j+2} + \hat{c}^\dagger_{2j+2}\hat{c}_{2j+1}\right)\right)\mathrm{e}^{-\mathrm{i}\lambda\hat{A}} + \hat{H}_A + \hat{H}_\Delta \\ &= -J_1\sum_j\left(\hat{c}^\dagger_{2j}\hat{c}_{2j+1}\mathrm{e}^{2\mathrm{i}\lambda} + \hat{c}^\dagger_{2j+1}\hat{c}_{2j}\mathrm{e}^{-2\mathrm{i}\lambda}\right) - J_2\sum_j\left(\hat{c}^\dagger_{2j+1}\hat{c}_{2j+2}\mathrm{e}^{-2\mathrm{i}\lambda} + \hat{c}^\dagger_{2j+2}\hat{c}_{2j+1}\mathrm{e}^{2\mathrm{i}\lambda}\right) + \hat{H}_A + \hat{H}_\Delta.\end{aligned} \tag{C.19}$$

List of Figures